Why Do Sudden Commencements Sometimes Generate Disproportionate Geomagnetically Induced Currents?

A. W. Smith[1], C. J. Rodger[2], K. M. Pratscher[3], D. H. Mac Manus[2], I. J. Rae[1], D. Ratliff[1], M. A. Clilverd[4], E. Lawrence [5], C. D. Beggan [5], G. S. Richardson [5], A. R. Fogg [6], D. M. Oliveira [7,8], J. Hübert [5], T. Petersen [9], M. Dalzell [10]

[1]Department of Mathematics, Physics and Electrical Engineering, Northumbria University, Newcastle upon Tyne, UK
[2]Department of Physics, University of Otago, Dunedin, New Zealand
[3]School of Chemical and Physical Sciences, Victoria University of Wellington, Wellington, New Zealand
[4]British Antarctic Survey, Cambridge, United Kingdom
[5]British Geological Survey, Edinburgh, United Kingdom
[6]Astronomy & Astrophysics Section, School of Cosmic Physics, Dublin Institute for Advanced Studies, DIAS Dunsink Observatory, Dublin, Ireland
[7]Goddard Planetary Heliophysics Institute, University of Maryland, Baltimore, MD, United States
[8]Geospace Physics Laboratory, NASA Goddard Space Flight Center, Greenbelt, MD, United States
[9]Department of Data Science and Geohazards Monitoring, GNS Science, Wellington, New Zealand
[10]Transpower New Zealand Limited, Wellington, New Zealand

Key Points:

- One minute magnetic data systematically underestimate the maximum rate of change of the magnetic field due to Sudden Commencements (SCs).
- We introduce an analytical SC model, allowing us to tighten the relationship between magnetic field and GIC ($r^2 = 0.93$).
- The amplitude of the magnetic field 'step' linearly scales with the modeled GIC, while the 'speed' of the change obeys a non-linear scaling.

Corresponding author: A. W. Smith, andy.w.smith@northumbria.ac.uk

Abstract

Geomagnetically Induced Currents (GICs) in grounded, conducting infrastructure (e.g., power networks) represent an important space weather hazard. GICs are driven by the changing magnetic field at the Earth's surface. Due to a sparsity of GIC measurements, the rate of change of the horizontal geomagnetic field (H') is often used as a proxy. We focus on one cause of large GICs: Sudden Commencements (SCs) caused by an increase in solar wind dynamic pressure. Despite appearing homogeneous in one-minute cadence magnetic field data, a systematic variation has been observed in the correlation with the resulting GIC, depending on the magnetic local time. We investigate two questions: (a) do the data capture SC morphology, and (b) are some SCs intrinsically linked to larger GICs?

We find that one-minute magnetic field measurements underestimate the maximum H', with systematic local time variation. We introduce an analytical model that describes the key components of an SC, the use of which strengthens the correlation between maximum H' and GIC during SCs ($r^2 = 0.93$).

We conduct synthetic experiments with our analytical SC model and the GIC and geoelectric field models of Southern New Zealand and the United Kingdom, respectively. We find that the modeled GIC and geoelectric field linearly scale with the "size" of the SC, and non-linearly with the "speed" of the magnetic change. Rotating the magnetic signature shifts the geoelectric field and GICs across the network. Forecasting the model parameters would enable robust forecasting of SC-related GICs.

Plain Language Summary

Adverse space weather can induce anomalous extra currents in power infrastructure, posing a risk to its safe operation and the provision of electricity to customers. These extra currents are rarely measured directly. Instead we often rely upon a proxy measurement for monitoring and forecasting, namely the changing ground magnetic field that ultimately causes the currents. While the currents have been shown to correlate strongly with the proxy measurement, there have been observations of systematic differences in the connection. We investigate these differences, showing that magnetic field measurements of a typical time resolution (one minute) do not capture the properties of the changing magnetic field during a key type of event. We create a simple model, showing that it well characterizes the magnetic field changes and their relationship with the induced currents. We then test how different "types" of magnetic event correspond to the currents, finding that the "rise time" of the event can change how effectively the magnetic change corresponds to the induced current.

1 Introduction

A key space weather hazard is the generation of large, anomalous "Geomagnetically Induced Currents" (GICs) in conducting infrastructure. Low resistance, high-voltage power systems are particularly vulnerable to GICs. Within a transformer such currents offset the hysteresis curve of the voltage cycle, which may lead to "hot-spots" that can damage the transformer. Further, saturation of the transformer core can distort the waveform, creating additional harmonics that can cause mis-operation and potentially trip safety measures (e.g., Boteler, 2003). Accurate prediction of large GICs would enable an infrastructure operator to take actions to mitigate GIC impact, potentially preventing damage and reducing associated societal costs by more than a factor of 10 (e.g., Oughton et al., 2019). Such a mitigation plans have been developed for New Zealand (Mac Manus et al., 2023), and were deployed during the large geomagnetic storm in May 2024 (the "Gannon storm", e.g., Grandin et al. (2024); Hayakawa et al. (2025)).

GICs are driven by the changing magnetic field at the surface of the Earth, in itself often caused by large, transient ionospheric current systems (approximately 100 km overhead). For example, at high latitudes the auroral current systems are critical, while at lower latitudes the equatorial electrojet is important. The link between the time-varying geomagnetic field and resulting GIC is complex, depending on the 3D conductivity of the solid Earth and the resulting induced geoelectric field (e.g., Beggan, 2015; Dimmock et al., 2019; Cordell et al., 2021), as well as the relative orientation and properties of the power network (e.g., Blake et al., 2018; Mac Manus et al., 2022). Precise translation requires computationally expensive modeling as well as detailed maps of the subsurface electrical conductivity over large regions, necessitating large-scale, expensive surveys. However, the one minute rate of change of the horizontal magnetic field, H (i.e., H') has long been used as a proxy for the GIC (Viljanen et al., 2001) - utilizing the assumption that larger rates of change of the geomagnetic field will be linked to larger GIC, for which (approximately linear) relationships have been demonstrated (Rodger et al., 2017; Mac Manus et al., 2017; Smith, Rodger, et al., 2022, 2024). This in turn has led to a large number of methods that attempt to forecast H' (e.g., Wintoft et al., 2015; Keesee et al., 2020; Madsen et al., 2022; Upendran et al., 2022; Pinto et al., 2022; Florczak et al., 2023), or when H' will exceed specific, high thresholds (e.g., Pulkkinen et al., 2013; Camporeale et al., 2020; Smith, Forsyth, Rae, Garton, et al., 2021; Coughlan et al., 2023). The rate of change of the magnetic field has also been used to statistically examine and estimate the magnitude of extreme events (e.g., Thomson et al., 2011; Rogers et al., 2020; Fogg, Jackman, et al., 2023; Wang et al., 2025). As such it is important to understand the uncertainties involved in the relationships between the peak H' and GIC.

Typically, H' is calculated using readily available one minute time resolution magnetic field data. The use of $60\,s$ data to calculate H' naturally smooths the data such that it reflects the nature of the induction process (Clilverd et al., 2020), however this sampling rate will preclude the inclusion of phenomena such as ULF (Ultra-Low Frequency) waves with periods smaller than $120\,s$ (Heyns et al., 2021; Hartinger et al., 2023), which may be a problem at lower latitudes: the frequency of such ULF waves is latitude dependent. Further, impulsive phenomena that manifest as rapid changes may not be well characterized by the "low" resolution $60\,s$ data: Sudden Commencements, for example (e.g., Smith, Rodger, et al., 2022).

Sudden Commencements (SCs) occur when the Earth's magnetic field is impacted by a rapid increase in solar wind ram pressure (for example, an interplanetary shock). This causes a sharp change in the magnetic field, as measured on the ground (Curto et al., 2007; Fiori et al., 2014). These rapid changes in the geomagnetic field can be related to large GICs in power networks. For example in 2001 a damaged transformer in New Zealand was later linked to an SC (Marshall et al., 2012; Rodger et al., 2017; Oliveira et al., 2018), while two power system failures in Sweden in 2003 were also later attributed to SCs (Pulkkinen et al., 2005). Understanding the link between SCs and GICs is therefore an important topic of study.

Over the last decade New Zealand has emerged as a serendipitous location for studying the link between surface geomagnetic field and GIC due to a relative abundance of GIC observations with contemporaneous magnetic field observations. First, Mac Manus et al. (2017) showed a very good average correlation between H' and the GIC recorded at transformers across New Zealand during geomagnetically active intervals. Rodger et al. (2017) then demonstrated that a high correlation between H' and GIC was observed during ~ 25 of the largest peak GICs in the 2010s, many of which were notably highlighted as being related to SCs. Analyzing one of the more "sensitive" transformers Smith, Rodger, et al. (2022) then showed that this was true more broadly, examining over 300 SCs, observing excellent correlations between the maximum H' and GIC ($r^2 > 0.85$). However, while the correlations were high the authors noted a systematic dependence of the relationship on factors such as the magnetic local time of New Zealand when the

SC occurred: SC that occurred when New Zealand was on the dayside of the Earth were linked to 30% larger GICs on average. This was hypothesized to be a result of the sub-minute resolution structure of the SC magnetic signature, and in addition to any day/night differences in SC disturbance magnitude (e.g., Tanaka et al., 2020). This raises two critical questions: (a) does the typical 60 s data sufficiently capture the SCs on the day/nightside of the planet, and (b) are some types of SC morphology inherently linked to larger GICs?

SCs represent a complex magnetic field signature on the ground, and a given solar wind structure (i.e., interplanetary shock) will generate a geomagnetic response that varies with both latitude and local time (e.g., Fiori et al., 2014; Smith, Forsyth, Rae, Rodger, & Freeman, 2021; Fogg, Lester, et al., 2023). The magnetic signature of an SC can be decomposed into two key components: the "D_L" and "D_P" components (e.g., Araki, 1994; Lam & Rodger, 2001; Piersanti et al., 2025). The D_L component, which dominates at low latitudes, is caused by the compression of the magnetopause and enhancement of the magnetopause current system. The D_L component typically resembles a step-like change in the horizontal magnetic field, maximizing at noon local time and decreasing towards midnight (e.g., Kokubun, 1983; Russell et al., 1992). Meanwhile the D_P component, whose impact maximizes at higher latitudes, is better described as a two-pulse magnetic field change, caused by the coupling of the magnetopause compression to shear Alfvén waves, resulting in the formation of "traveling convection vortices" in the higher latitude ionosphere (Friis-Christensen et al., 1988). Piersanti and Villante (2016) developed a method to separate the two contributing factors that combine to create an SC, using the magnetic signature recorded by spacecraft in geosynchronous orbit - allowing the estimation of the isolated compressional D_L component. Once the estimated D_L component is subtracted it allowed the estimation of the ionospheric current flow patterns, with results found to be mostly consistent with theoretical expectations (i.e., Araki, 1994).

In this study, we examine how properties of the high resolution magnetic field signature of an SC impact the GIC or geoelectric field that will be observed, investigating precisely what makes an SC generate a larger than expected GIC, given the "size" of the magnetic signature as recorded with one-minute resolution data. We first introduce a general analytical model for SCs, demonstrating that this permits a superior estimation of the GIC that will be observed. We then statistically examine properties of the model SC and how they link to GIC, performing synthetic tests using the analytical magnetic field model and detailed 3D models (Hübert et al., 2025; Pratscher et al., 2024). We then discuss our results in the context of local time, geology and the implications for space weather forecasting.

2 Data

In this study we primarily compare magnetic field and GIC data from New Zealand. We use magnetic field data from the Eyrewell (EYR) magnetometer station, located near Christchurch, New Zealand. We compare and contrast data recorded with one minute and one second cadence (GNSScience, 2022). We principally work with the rate of change of the horizontal magnetic field (H'), where the horizontal field is defined as $H = \sqrt{X^2 + Y^2}$ (X and Y being the North and East components of the horizontal magnetic field respectively). Further, we normalize the data such that the units are nT min^{-1} for both the one minute and one second cadence data.

Between 2021 and 2022 a large-scale magnetotelluric (MT) survey was performed in Southern New Zealand (Ingham et al., 2023). In total, 62 sites across Otago and Southland were surveyed, separated by approximately 25 km (see Figure 1 of Pratscher et al. (2024)). Each survey sampled electric and magnetic field at a cadence of 1 s, allowing the estimation of impedance tensors across a wide frequency range. These impedance tensors permit the accurate estimation of geoelectric fields (and GIC), and have been shown to outperform more typical thin-sheet modeling particularly during SCs (Pratscher

et al., 2024). For details of the modeling process (e.g., from time varying magnetic field to GIC) and magnetotelluric measurements, the interested reader is directed to Pratscher et al. (2024). Importantly for our study, we assume no spatial variation of the magnetic field across the model domain, and where the model is driven by magnetometer data we use that available from the EYR observatory (at a distance of several hundred km).

The magnetic field data are complemented by GIC observations from Transformer T2 at the South Dunedin (SDN) substation. This transformer was selected for several reasons. First, it is located within the spatial region covered by the recent high resolution magnetotelluric survey (Ingham et al., 2023). Second, it has been shown to be sensitive to SC events in the past, i.e., shows a relatively strong, clear GIC response to SCs (Mac Manus et al., 2017; Smith, Rodger, et al., 2024). Third, it has been monitored for a sufficient length of time to permit this study. We use the GIC data at SDN T2 both to explore relationships between H' and GIC, and to validate our modeling and synthetic experiments. A detailed description of the method by which the GIC data are derived can be found in Mac Manus et al. (2017), while Clilverd et al. (2020) describe how the data are recorded: if the data are dynamic (i.e., changing by more than $0.2\,$A) then the data are recorded at a cadence of $4\,$s, with a slower cadence at other intervals.

We investigate 20 SCs from between 2011 and 2016, listed in the table within Appendix A. These 20 events were selected from the much larger list employed by Smith, Rodger, et al. (2024), which comprised 232 SCs between 2001 and 2020. This list was originally derived through use of the ShockSpotter method using SOHO data from L1 (https://space.umd.edu/pm/), before being limited to those for which a corresponding ground signature was present at EYR in New Zealand. The limited subset of 20 SCs was then selected based on several considerations. First, these events show clear, well defined magnetic field signatures at EYR within which D_L and D_P components could be estimated, whilst covering the full range of magnetic local times. Second, these events occurred during a period within which high resolution (one second) magnetic field data are available from the EYR observatory, and for which GIC data were routinely recorded in South Dunedin.

The focus on New Zealand is complemented by a comparison to the United Kingdom, at a similar geomagnetic latitude. In the UK 14 MT sites were sampled between 1990 and 2020, predominantly in Southern Scotland, along with the three permanent observatories. These were later extended by a campaign between 2020 and 2024 which added an additional 53 locations to cover most of the UK (including Shetland) (Huebert et al., 2024).

3 Results

First, we examine whether the $60\,$s data is adequately capturing the magnetic signature of the SC, and whether this could depend on magnetic local time - contributing to the previously reported results (Smith, Rodger, et al., 2022, 2024).

3.1 Example Sudden Commencements

Figure 1 shows six example SCs to illustrate the range of magnetic field observations made during an SC, along with the corresponding GIC measurements made at SDN T2. For each event an arbitrary baseline (H_0) has been subtracted to make the magnitude of each event more comparable. The six SCs are arranged by magnetic local time (MLT), with noon to the top of the figure, the red dots then connect and identify the MLT on a schematic of the Earth in the center. From inspection of the six SCs we can see the complex interplay between the step-like "D_L" component and twin pulse "D_P", and further that these vary event-to-event. The interested reader is also directed to Piersanti
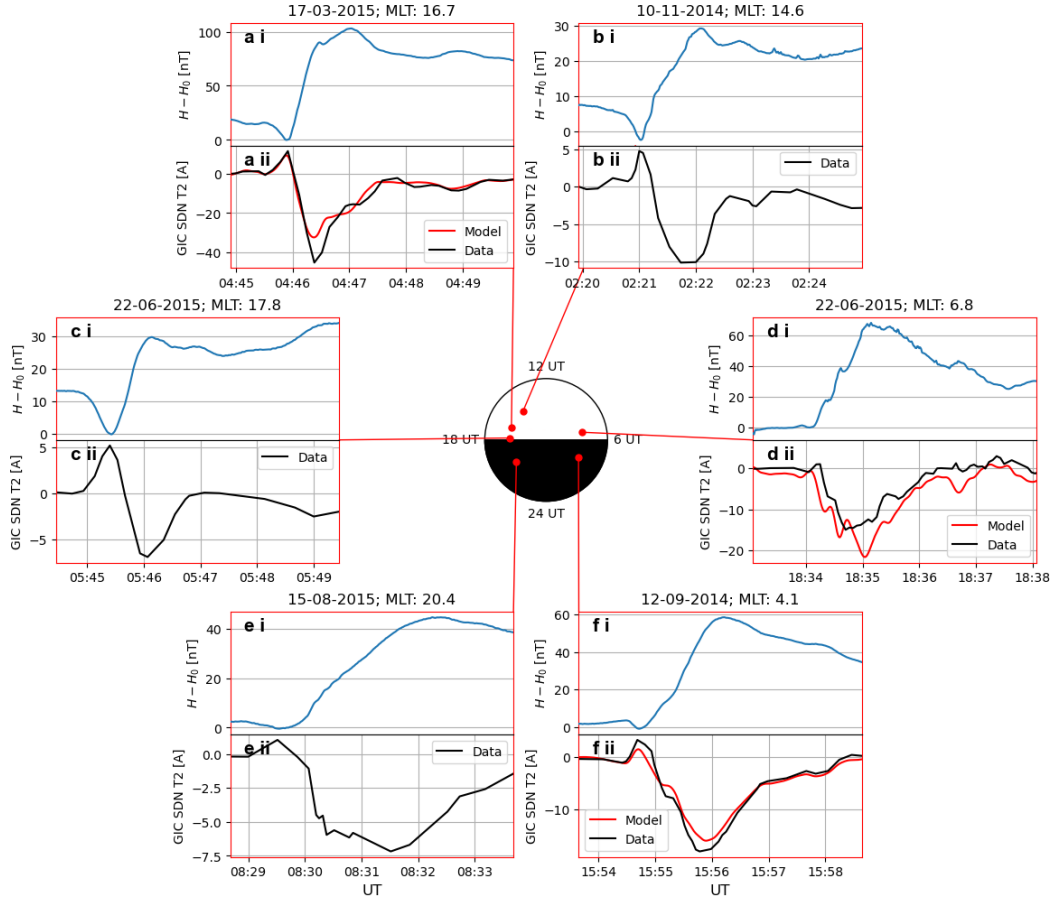
Figure 1. Magnetic field and GIC observations for several minutes during six example SCs. The magnetic field observations at 1 s cadence are taken from EYR (upper panels, i), while the GIC measurements are from SDN T2 (lower panels, ii, in gray). We also show the predicted GIC obtained from using the magnetic field observations at EYR and the MT modeling in red (e.g., Pratscher et al., 2024) for three test events (a, d and f). The center panel illustrates a polar view of the Earth, with the magnetic local time of the observation given by the location of the corresponding red dot on the "Earth", while the distance from the center is the same for all points.

et al. (2025), who detail how the morphology of a single SC changes with MLT and latitude, using multiple magnetometer stations across the globe.

Broadly, we see that events Figure 1a - c show strong, almost sinusoidal D_P contributions, with a leading negative impulse, as suggested by Araki (1994) in the afternoon sector. By eye, Figure 1d has a less clear D_P contribution, but this could be an example where the D_L contribution dominates. On the nightside, we see that the SCs in Figure 1e and f show little to no evidence of significant D_P components, as expected (Moretto et al., 2002).

Regarding the step-like D_L component we see that on the dayside (e.g., Figure 1a and b) the step occurs relatively rapidly, taking around one minute at most. In contrast on the nightside (e.g., Figure 1e and f) the change is more gradual, taking two or three minutes to reach its peak. Some of this apparent behavior may be due to the consider-

able D_P component on the dayside, but without disentangling these contributions it is not possible to definitively ascribe the behavior, e.g., Figure 1c. Such disentanglement can typically be achieved through the use of empirical magnetic field models and geosynchronous magnetic field observations (e.g., Piersanti & Villante, 2016), or global numerical models that can distinguish the magnetospheric and assorted ionospheric contributions (e.g., Tanaka et al., 2020; Kikuchi et al., 2022; Fujita & Tanaka, 2022).

The observed GIC at SDN T2 (dark gray in lower panels of Figure 1) can be seen to effectively mirror the magnetic field changes observed at EYR, with both the D_L and D_P components contributing to the GIC (e.g., Figure 1c). More detailed comparisons will be performed below. In Figure 1 we also show the results of modeling the GIC at SDN T2 during three test SCs, using the magnetic field at EYR as input and the MT impedances from Pratscher et al. (2024) in red. As reported by Pratscher et al. (2024), we find an excellent correspondence between the modeled and observed GIC. Small differences in this comparison could be a result of the spatial offset between the magnetometer observations at EYR (midway up the South Island) and region of interest (lower South Island).

3.2 Correlation between Maximum H' and GIC

In New Zealand the rate of change of the horizontal magnetic field (H') has been found to correlate well with the observed GIC during active periods (Mac Manus et al., 2017), during the largest GIC peaks (Rodger et al., 2017), and specifically during SCs (Smith, Rodger, et al., 2022, 2024). Figure 2 shows the correlation between the peak GIC recorded at SDN T2 and the contemporaneous peak H' at EYR recorded in (a) 1 minute and (b) 1 second resolution data. Though with only 30% of the events of the wider statistical study performed by Smith, Rodger, et al. (2024), both the gradient of the correlation and r^2 values are consistent with the previous analysis at one minute resolution (Figure 2a).

If we move from one minute to one second resolution data (i.e. from Figure 2a to b), attempting to capture the sub-minute features displayed in Figure 1, we find that the correlation (r^2) weakens, dropping from 0.85 to 0.65. The gradient of the correlation also reduces: the one minute data underestimates the maximum H' during the SC (from the perspective of the 1 s data). Rodger et al. (2017) showed a similar but more dramatic deterioration in correlation moving from one minute to one second data, albeit with a sample selected through large H', only some of which were related to SCs. This was inferred to be due to the impact of high frequency noise in the one second cadence data and the fact that one second variation will not induce a geomagnetic field at depth.

To explore the impact of moving to a higher time resolution, Figure 3 shows two example SCs at both data resolutions. Both events show SCs with a clear D_P ("twin-impulse") component, while the step-like D_L component is clearly stronger in the SC that occurred in March 2015 (Figure 3a, left panels). The contemporaneous GICs recorded at SDN T2 clearly show evidence of the higher time resolution features, i.e., those missing from the 60 s data. Nonetheless, it is broadly true that a larger maximum rate of change is recorded for the March SC (left) than the June SC (right), and the corresponding maximum GICs follow the same pattern.

In Figure 3a (i) we see that while the 60 s data appears to capture the broad step of the SC, it underestimates the rate of change by a factor of four (Figure 3a ii). H' is certainly highly variable in Figure 3a ii, but the largest change during the SC is consistent, and not an artifact. Meanwhile in the June SC (Figure 3b ii), we see that the strong D_P signature, and resulting "double hump" in H', is not captured at all with the lower time resolution (60 s) data - leading to an underestimate of H' of around a factor of five. The 60 s data is clearly not capturing key structures of the SC magnetic signature. The
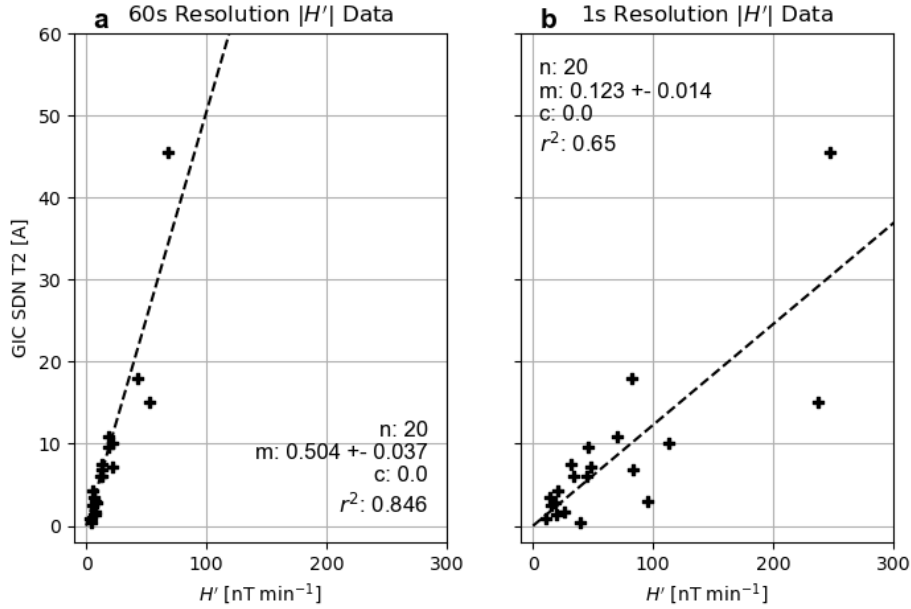
Figure 2. The correlation between the maximum H' at EYR and the peak GIC recorded at SDN T2. We show this for the (a) 60 s cadence and (b) 1 s cadence magnetic field measurements. The black dashed best fit lines are linear fits obtained from orthogonal distance regression, constrained to have an intercept of zero.

underestimation of H' in the 60 s data by factors of four or five is consistent with the statistical results shown in Figure 2.

While the maximum H' may be a good proxy for the maximum GIC during SCs ($r^2 = 0.85$, with our one minute sample), the rate of change (H') implicitly applies a band-pass filter on the data which limits the frequency content it can capture (and depends on the resolution of the data). Alternative proxies do exist, for example proxies of the geoelectric field (e.g., Marshall et al., 2010; Piersanti et al., 2019), such proxies often involve filtering and processing in the Fourier domain, and some require knowledge of the electrical conductivity of the subsurface (i.e., Piersanti et al., 2019). The focus in this study is on H' as it represents the most common proxy for GICs, however in Appendix B we compare the application of the GIC Indices tested by Marshall et al. (2011). This method is chosen as these indices do not require additional information as to the sub-surface conductivity and as such are universally applicable, however we note that this will be a source of uncertainty in the proxy. These GIC indices are shown to provide good proxies for the GIC at SDN T2, comparable to H' in this case ($r^2 = 0.87$).

3.3 Analytical SC Model

While the 1 s data captures the essential, sub-minute features of the magnetic signature of the SCs it is likely that the inherent noise in the data precludes its reduction to a simplistic metric (i.e., maximum H'). A simple choice to overcome this would be to low-pass filter the time series data to a lower effective resolution, 10 s for example (c.f., Bower et al., 2024). However, we can instead turn to the physics of the magnetic signature and create a simple analytical model, enabling us to then probe the coupling of the magnetic signature to the solid Earth and resulting GIC. This model replicates the two
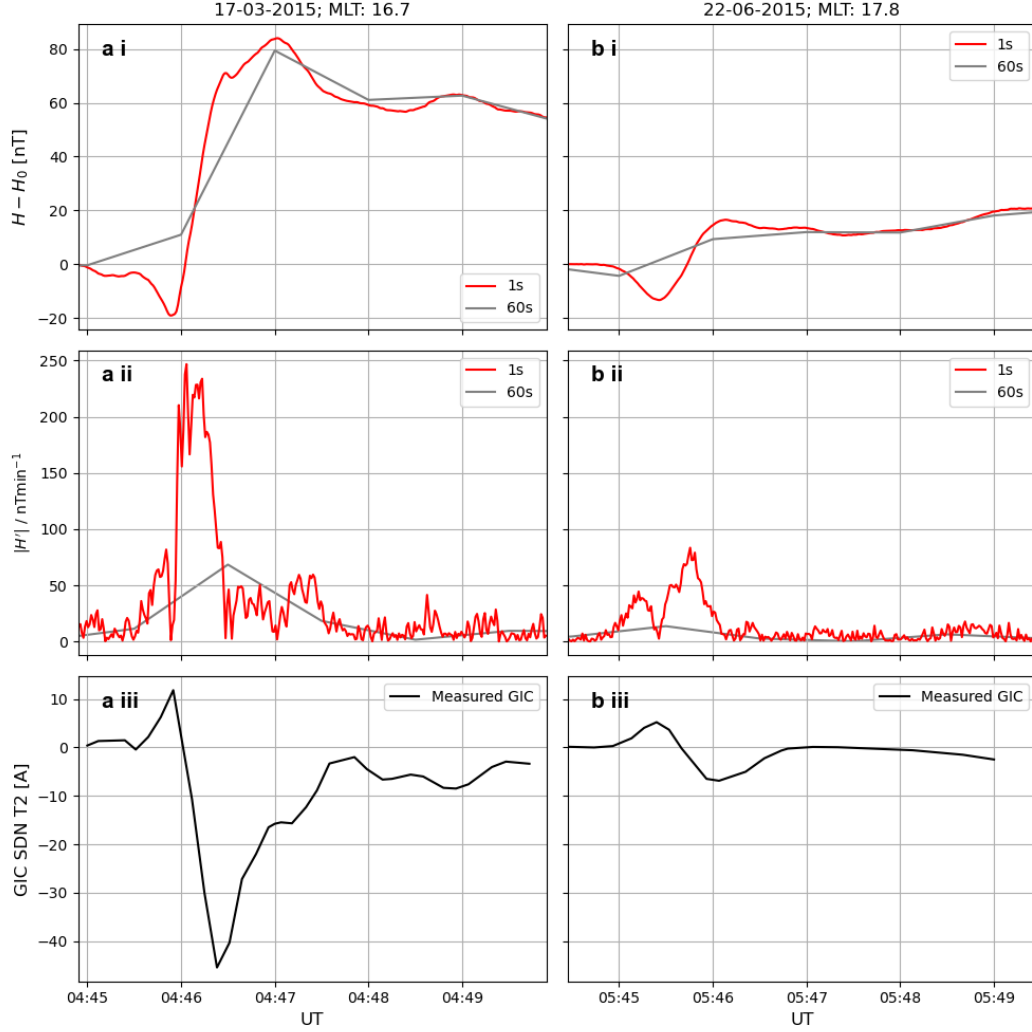
Figure 3. Five minute intervals around two example SCs (a and b, left and right respectively). The top two panels show magnetic field data recorded at EYR at one minute resolution (blue) and one second resolution (red). The top panel (i) shows the background subtracted horizontal component of the magnetic field, while the middle panel (ii) shows the absolute rate of change of the horizontal magnetic field (first difference) derived from panel (i). The third panel (iii) shows the GIC measured at SDN T2 for the same interval.

key contributors to the magnetic signature of the SC, namely the D_L and D_P components:

$$D_L(t) = A_{DL} \tanh\left(\omega(t - t_0)\right) + A_{DL} \tag{1}$$

$$D_P(t) = A_{DP} \cos\left(\frac{2\pi(t - t_1)}{\tau} + \phi\right) \exp\left(\frac{-(t - t_1)^2}{\sigma^2}\right) \tag{2}$$

where A_{DL}, ω, t_0, A_{DP}, t_1, τ, and ϕ represent free parameters to be determined. We set σ to $^\tau/_\pi$ to preserve a two-impulse structure. Equations 1 and 2 give the SC perturbation of the horizontal magnetic field. However, these functional forms are fit to the B_X (North) and B_Y (East) components of the magnetic field, and so we introduce two additional parameters θ_{DL} and θ_{DP} to deconvolve the horizontal magnetic field into its components.

For the D_L component, the critical parameters are A_{DL} and ω, which correspond to the "size" and "speed" of the step-like magnetic field change. The D_L signature is largely a result of the increasing Chapman-Ferraro magnetopause current system. Meanwhile, for the D_P component which describes the impact of transient ionospheric current systems, the A_{DP}, τ and ϕ parameters are key. These represent the "size" of the D_P signature, the temporal width of the two-pulse signature, and the relative size of each pulse (the preliminary and main impulses: Araki (1994)).

This model has a total of nine free parameters, representing a challenge to converge to a global, physics-informed minimum. In this study we use the emcee Python fitting package (Foreman-Mackey et al., 2012), which has heritage in the field (e.g., Smith et al., 2018; Fogg, Jackman, et al., 2023). We also note that the fit must be manually initiated at a good starting point, or the high dimensional model can converge to an unlikely or nonphysical fits. This is a downside of this method when compared to those such as that employed by Piersanti and Villante (2016), which use observations in geosynchronous orbit to estimate the D_L component directly. However, the benefit is that no other models (e.g., empirical magnetic field models) or data (e.g., from geosynchronous satellites) are required.

Figure 4 shows two examples of analytical model fits, to the same SCs shown in Figure 3. The top panels show the fit to the H component of the magnetic field, while the middle shows the resulting fits to the rate of change of the horizontal field (H'). The bottom panels show the resulting GIC recorded at SDN T2 for context and ensuring the format is familiar from Figure 3. The D_L and D_P components from Equations 1 and 2 are shown in orange and green respectively, while the total model fit is in blue. For both of the events in Figure 4 we can see that the model captures the key morphological features in both H and H', despite not being directly fit to either time series.

3.4 Reanalysis of Maximum H' and GIC

The first result enabled by the model fitting above is the reanalysis of the correlation between maximum H' and GIC during the events. Figures 5a and b repeat the previous results of Figure 2, this time with a color bar indicating the magnetic local time (MLT) of New Zealand during the SC. The color of the points in Figure 5a shows no clear ordering (i.e., above and below the line of best fit), suggesting that the correlation between the maximum observed H' (evaluated at 60 s time resolution) and GIC measured at SDN T2 shows little or no dependence on MLT, in contrast to other locations in New Zealand (e.g. Smith, Rodger, et al., 2024). This may be a result of the local geology or geometry of the power network.
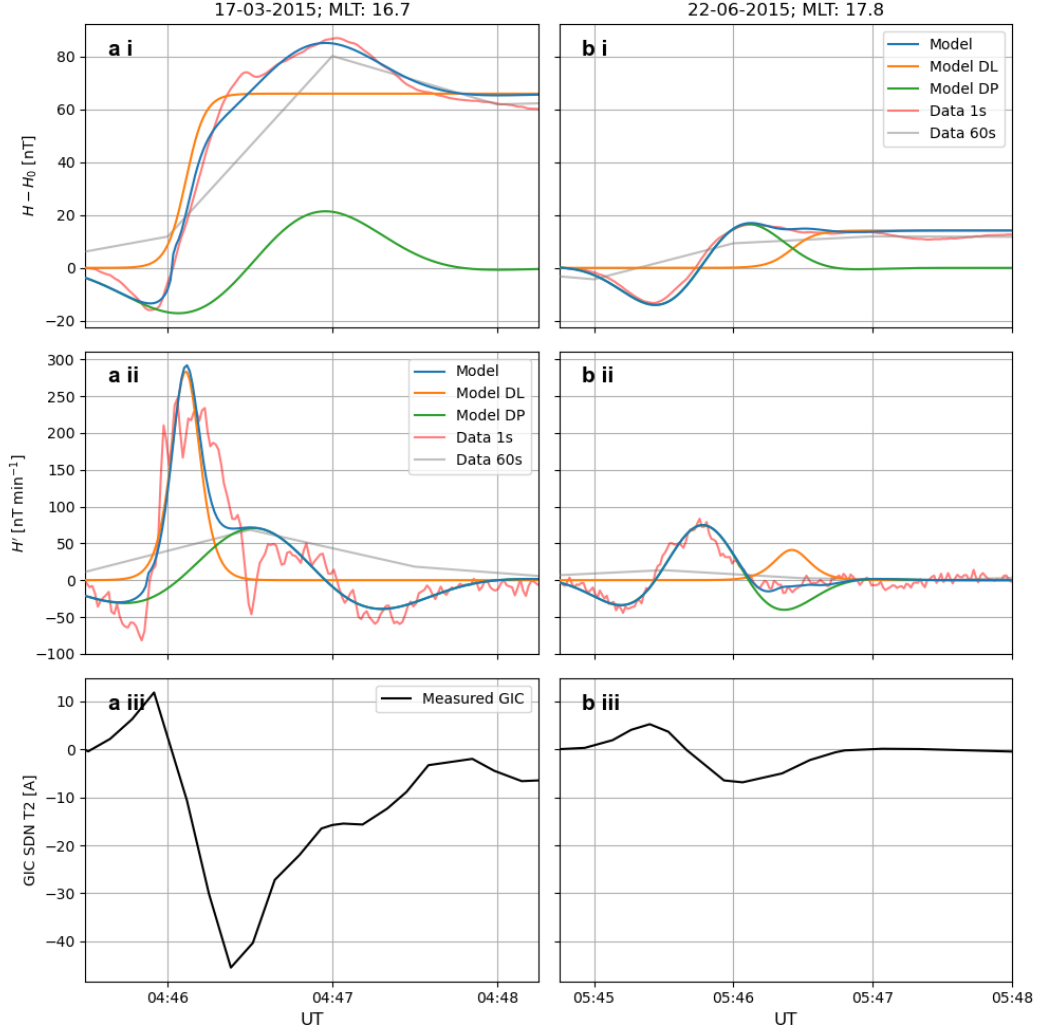
Figure 4. The two example SCs from Figure 3 (a and b). The top panel (i) shows the background subtracted horizontal magnetic field (H), while the middle panel (ii) shows the rate of change of the horizontal magnetic field (H'). The red and gray represent the two different resolutions of magnetic field data (1 s and 60 s, respectively) while the orange and green represent the two components of the analytical model (DL and DP, respectively). The blue shows the final total analytical model fit. The lower panel (ii) shows the GIC recorded at SDN T2.
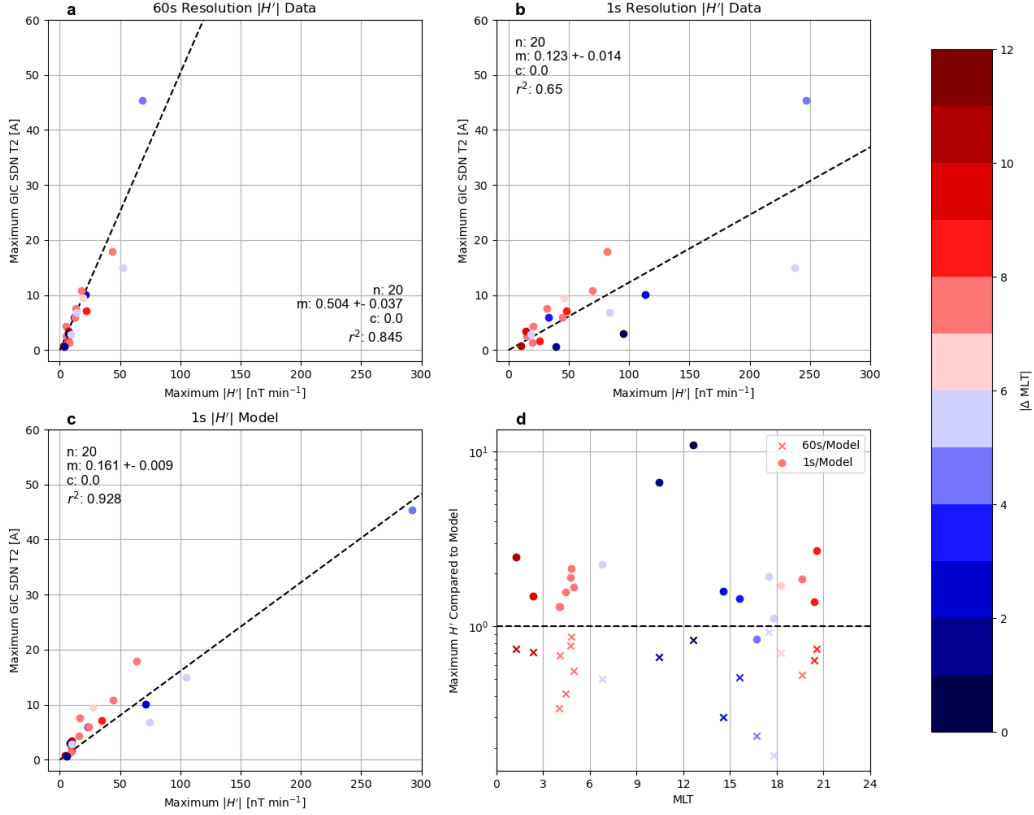
Figure 5. A detailed reanalysis of the correlation between the maximum H' and GIC during the 20 SCs. The correlation is shown for H' derived from 60 s cadence magnetic field data (a), 1 s cadence data (b), and the maximum H' extracted from the fitted analytical model (c). The final panel (d) shows the ratio of maximum H' extracted from the 60 s (crosses) and 1 s (dots) data compared to the analytical model. The color here indicates the longitudinal distance from local noon, measured in hours. Blue indicates the event occurred when New Zealand was on the "dayside" while red indicates that New Zealand was on the "nightside".

As above, when moving to 1 s data we see a weakening of the correlation between the maximum observed H' and measured GIC (Figure 5b). On further inspection of Figure 5b we can start to see a pattern, where those SCs that occurred when New Zealand was closer to local noon (i.e. colored blue) seem to more often have a larger estimate for the maximum H', i.e., are often located below the line of best fit. This may indicate a greater contribution from high frequency, sub minute noise at "daytime" local times, though with a very small sample size.

When we move to the correlation from the model-derived maximum H' (Figure 5c, e.g., the maximum H' derived from Figures 4 a and b ii) we see that the correlation (r^2) has increased markedly, compared to both the 1 s and 60 s cadence derived quantities (Figures 5 a and b). However, we still see a remnant pattern where dayside (blue) SCs require larger H' for a given GIC to be observed, i.e., the dayside SCs are located below the line of best fit.

Investigating the impact of MLT on the changing correlation, Figure 5d shows the difference in maximum H' between that obtained using the analytical model and the 1 s and 60 s data (dots and crosses, respectively). In this figure, the data derived maximum H' are divided by that produced with the model, therefore the horizontal dashed line indicates equality: deviations from this show where the high (e.g., one second) and low (e.g., one minute) resolution data estimations differ from that obtained with the analytical model. While for some SCs the estimates only differ by $\sim 10\%$, for some the estimates of H' are different by a factor of 10. Albeit with a small sample size, the one second data-derived maximum H' seem to be most different at local noon, while the estimates derived from the 60 s data are most likely to underestimate the rate of change of the magnetic field moving from noon around to dusk. Importantly for previous studies, it seems consistent that the 60 s data may give lower estimates for the maximum H', and this effect is most pronounced on the dayside. Assuming an idealized perfect correlation between the maximum H' and GIC, this effect may explain the apparent ability for dayside SCs to generate disproportionately large GICs for their given H' (c.f. Smith, Forsyth, et al., 2022; Smith, Rodger, et al., 2024).

3.5 Testing Model Parameters

As highlighted above in Figure 5c, after "controlling" for data resolution at SDN T2 there is a tendency for SCs that occur when New Zealand is on the dayside to be linked to smaller GICs, for a given H' (i.e., the blue points are mostly below the line of best fit). Each parameter of the SC model will be driven by some combination of the properties of the incident interplanetary shock (e.g., Oliveira, 2023), the location of the observation both in MLT and MLat, and the local geological properties (Tanskanen et al., 2001). In this case, we assume that a fundamental component of the SC magnetic signature depends on MLT, and that is leading to the difference observed. The analytical model allows us to examine the properties of each SC, with the parameters described in Section 3.3. Figure 6 shows the relationship between the maximum H' (inferred from the analytical model fit) and the maximum GIC recorded at SDN T2, as in Figure 5c, with the color in each panel indicating one of the key model parameters.

We would expect that the size of the maximum H' will scale with several of the parameters tested in Figure 6, e.g. the amplitude of the D_L component (A_{DL}), given the form of Equation 1. For this reason, we are most interested in parameters that appear to vary from top left to bottom right (i.e., give a larger/smaller GIC for a fixed maximum H'), rather than parameters that vary from bottom left to top right (e.g., where both maximum H' and GIC are increasing). We also highlight that within Figure 6 the four largest events (by maximum H') that lie beneath the line of best fit (black dashed line) occurred on the dayside (e.g., Figure 5). With these two considerations, we note that ω (Figure 6c) and A_{DP} (along with A_{DP}^{Max}) (Figure 6e) perhaps show larger values
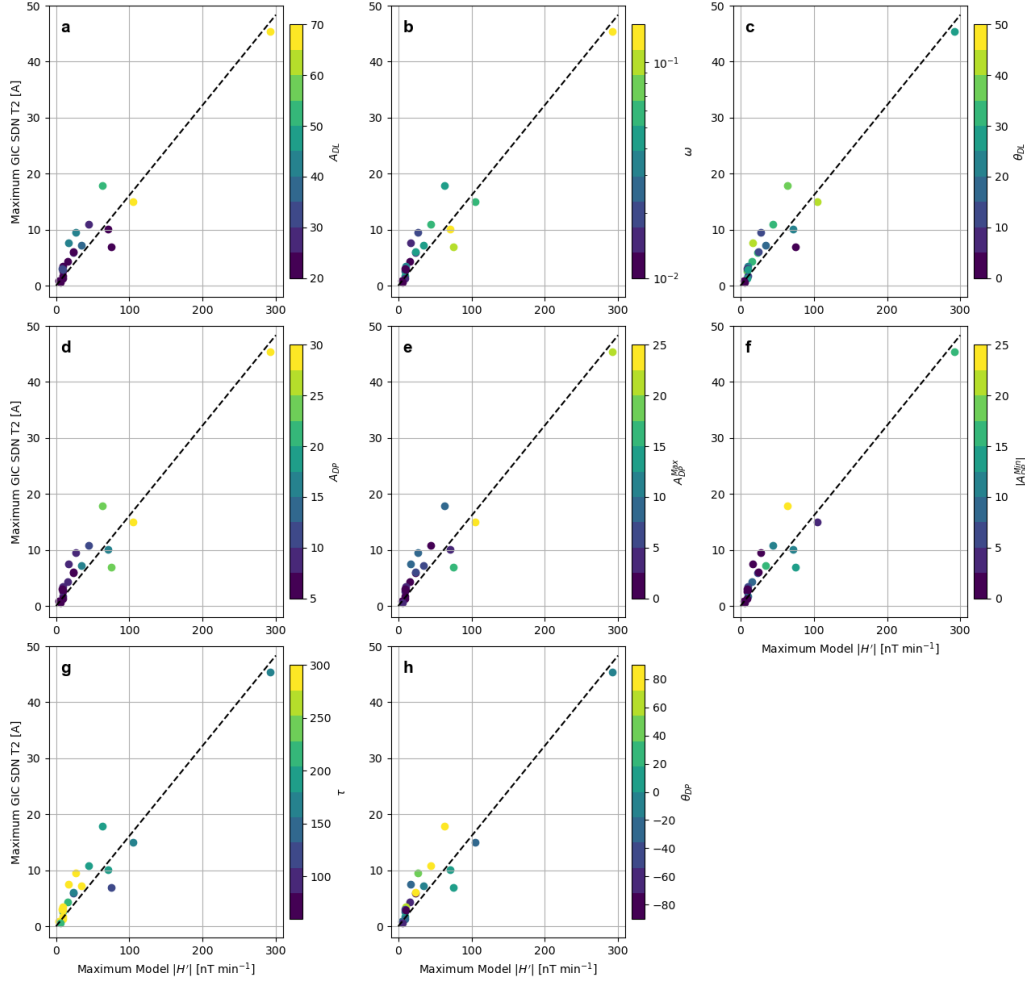
Figure 6. Examining the variation of several analytical model parameters with MLT. Each panel displays the relationship between the maximum H' (derived from the analytical model fit) and the maximum GIC observed at SDN T2. The color scale for each panel then illustrates the value of several key parameters of the analytical model: (a) A_{DL}, (b) ω, (c) θ_{DL}, (d) A_{DP}, (e) A_{DP}^{Max}, (f) A_{DP}^{Min}, (g) τ, and (h) θ_{DP}. The black dashed line indicates the line of best fit (determined through Orthogonal Distance Regression, ODR).

in events below the line of best fit. Therefore it is possible that SCs linked to faster rise times (larger ω) or with stronger contributions from the D_P component (i.e., larger A_{DP}) are preferentially linked to smaller GIC for a given H', though with a small sample size. The trends in other parameters are less clear, though τ (i.e., pseudo-period of the D_L perturbation) may also show an interesting trend with shorter effective periods leading to smaller relative GICs.

4 Synthetic Model Tests

Figure 6 may suggest why some SCs may show preferential "coupling" to the GIC recorded at some locations: namely, several parameters of the analytical model appear to be systematically linked to smaller relative GIC at a fixed maximum H'. We now ex-

ploit the power of the analytical model to run a series of synthetic experiments. As our baseline SC we use an event that occurred on 22nd June 2015, at around 18:30 UT (around 12 hours after the event on the right of Figures 3 and 4). This event was selected as it showed clear D_L and D_P contributions and was very well described by the analytical model ($r^2 = 0.97$).

4.1 Synthetic Model Results at SDN T2

To start, we begin by considering solely the SDN T2 transformer, as above. Figure 7 shows three tests, targeting three different parameters of the analytical model. First, we select A_{DL} (Figure 7a) as it is of interest to see what would happen if the size of the magnetic signature is increased, and in particular how this corresponds to the observed GIC. Further, the size of the step-change in D_L has been suggested to be directly related the square root of the change in dynamic pressure observed during the interplanetary shock (e.g., Siscoe et al., 1968; Su & Konradi, 1975; Araki et al., 1993; Russell et al., 1994; Shinbori et al., 2009). Second, ω (Figure 7b) was selected as it was highlighted above as a parameter that may vary with MLT and could explain the tendency in Figure 5 for dayside SCs to generate smaller relative GICs (for a given maximum H'). Third, we test θ_{DL} (Figure 7c), effectively rotating the D_L component of the SC from B_X through to B_Y as this strongly changes the magnetic field signature in two-dimensions but retains a similar H perturbation. This would alter the way in which the magnetic change interacts with the geology and power network. We note that we focus on parameters of the D_L component of the SC signature as it is found to be clear for all events, in contrast to the D_P component which is mostly present in limited MLT sectors.

The GIC reported in Figure 7 was modeled using the magnetotelluric survey of Ingham et al. (2023), consisting of 62 sites covering the South of the South Island of New Zealand, and a detailed model of the power network, as in Pratscher et al. (2024). The magnetic input to this model are shown in the top two rows of Figure 7 (B_X and B_Y), and we note that we assume no spatial variation in the magnetic signature across the model domain. Within Figure 1 we showed that we can accurately replicate the GIC within this region, solely relying on the magnetic field data recorded at EYR, several hundred kilometers North of the model domain, therefore this is not an unreasonable assumption.

For the A_{DL} test (Figure 7a), we see the three (semi-arbitrarily chosen) values of A_{DL}: 10, 34.5 and 55 in blue, orange and green respectively. In the top two panels we see a significant magnetic signature in both B_X and B_Y, though the D_P signature appears more strongly in B_X. This is due to the orientation of the D_L and D_P components in the original "template" SC on 22nd June 2015. In H and H' (Figure 7a iii and iv) we see that both scale with increasing A_{DL}, with approximately linear increases in both H and H'. In the resulting GIC (Figure 7a v) we also see an increasing GIC observed with increasing A_{DL}, with what appears to be an approximately proportional increase in GIC.

Regarding the speed of the rise of the D_L component (ω) we again test three possible values, increasing from 0.015 to 0.055 to 0.1 (Figure 7b). These values were selected based on the range of possibilities observed in the 20 SCs within the study. This changing "slope" of the D_L component is most clear in B_Y, where the lower contribution of D_P shows that the 0.015 (blue) test SC clearly has a slower rise than the other two synthetic test SCs. The differences between the three tests are also relatively clear in H (Figure 7b iii), though the difference between the 0.055 and 0.1 tests (green and orange) look to be less major. However, that is only until we consider H' (Figure 7b iv), where the largest ω clearly results in a short, sharp peak. When assessing the resulting GIC (Figure 7b v) there is still a clear progression with increasing maximum GIC with increasing ω (i.e., blue to orange to green), but it appears less pronounced than the previous A_{DL} test.
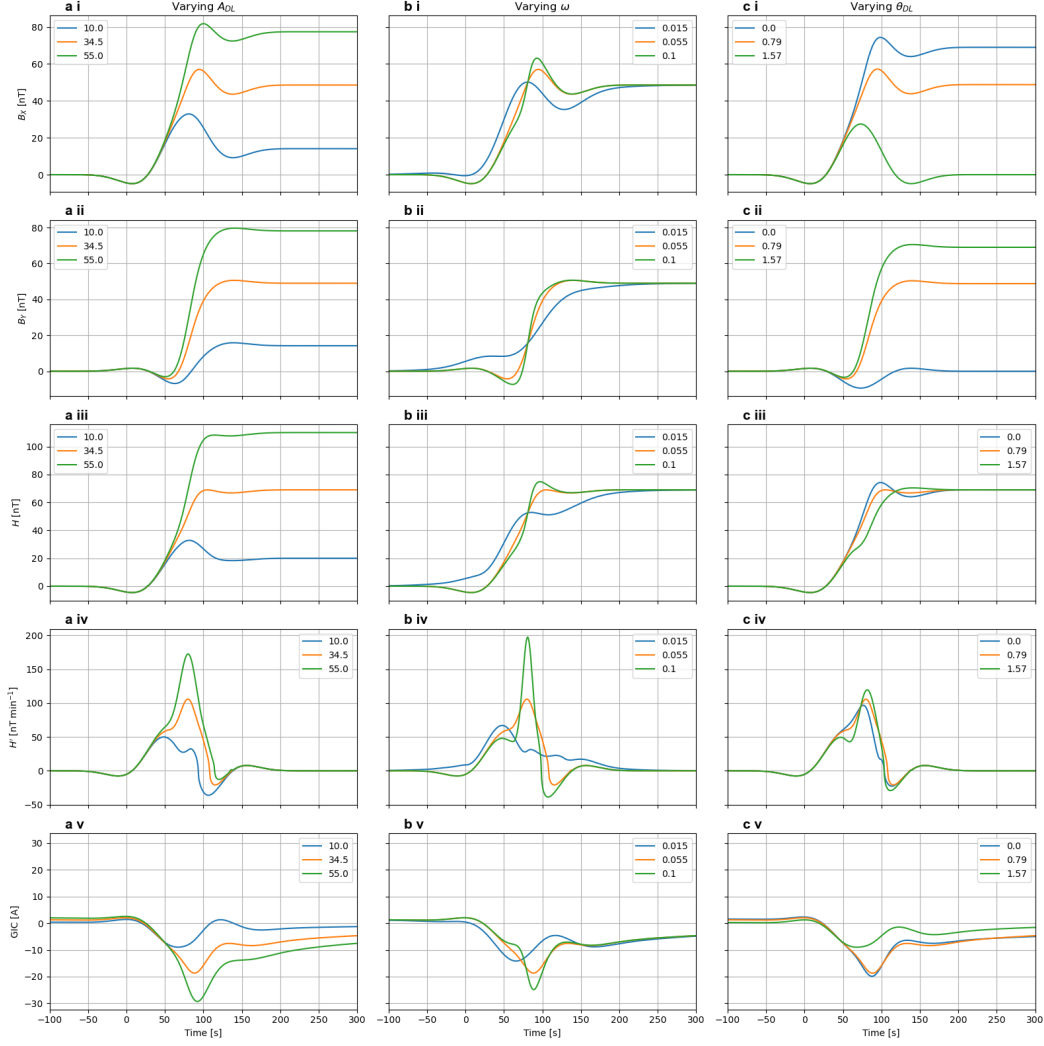
Figure 7. Three synthetic model tests for the parameters A_{DL} (left, a), ω (center, b), and θ_{DL} (right, c). Each row shows a different, linked facet of the model test: B_X (i), B_Y (ii), H (iii), H' (iv), and the modeled GIC at SDN T2 (v). The orange indicates the original analytical model fit to an SC on 22nd June 2015 ($\sim$ 18:30 UT). The green indicates a synthetic test where the respective parameter (given by the column) is increased in value, while the blue indicates a test where the parameter has been reduced. The GIC in SDN T2 has been calculated using the MT impedances, similar to Pratscher et al. (2024).
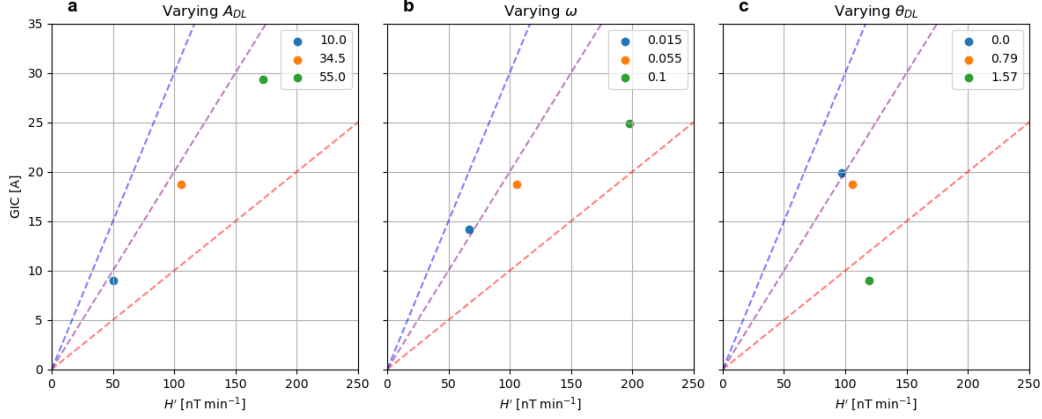
Figure 8. The correlation between the maximum H' and maximum GIC calculated during the synthetic test SCs in Figure 7. The three columns indicate the tests regarding the three different model variables: A_{DL} (a), ω (b) and θ_{DL} (c). The dashed blue, purple and orange lines indicate three arbitrary linear relationships to guide the eye.

The final test was rotating the D_L component using θ_{DL} (Figure 7c). The test begins with the D_L component solely in the X (North) direction (blue), rotating through 45° (orange), before being an East-West perturbation (green). We can clearly see this progression in Figure 7c i and ii, where the "step" rotates from the B_X to B_Y components of the field change. However, when regarding H and H' (Figure 7c iii and iv), as expected we do not see very large differences at all. The resulting GIC for this test (Figure 7c v) shows almost no difference between the tests where D_L is Northward or at 45° (blue and orange), but shows a large relative decrease when θ_{DL} is oriented in the East-West orientation. This must be due to the influences of the local geology and the relative geometry of the power network around SDN T2.

We now extract the maximum H' and GIC from the synthetic tests in Figure 7, effectively replicating the correlation analysis in the previous section, but this time from the synthetic tests rather than the observed data. Figure 8 shows the results for the three different model parameter tests, with arbitrary linear relationships marked with dashed lines to guide the eye.

For the first amplitude test (Figure 8a) we see that increasing A_{DL} increases the H' and calculated GIC proportionally: the tests would lie approximately along the same line (i.e., with the same gradient). In this case the relationship between H' appears to be approximately preserved by changing A_{DL}. With the second test (Figure 8b), we see that increasing ω does increase H', as above in Figure 7, however the GIC associated appears to diminish: a given increase in H' will result in a smaller increase in GIC. Finally, rotating the D_L signature via changing θ_{DL} (Figure 8c), can be seen to give a very small change in this correlation plot (i.e., blue to orange, $\theta_{DL} = 0$ to $^\pi/_4$) until the change is to a purely East-West orientation (i.e., $\theta_{DL} = {}^\pi/_2$, green) at which point the resulting GIC diminishes dramatically.

To show the relationships more clearly, Figure 9 shows the gradients (i.e., $^{GIC}/_{H'}$) as a function of model parameters (i.e., A_{DL}, ω, θ_{DL}). Figure 9a shows the previous inference that as A_{DL} increases the associated maximum H' also increases. Further, when the maximum H' is compared to the maximum resulting GIC (Figure 9d), we see that the relationship between the two is approximately constant: with approximately 0.18 A recorded for every additional H' (nT min^{-1}).
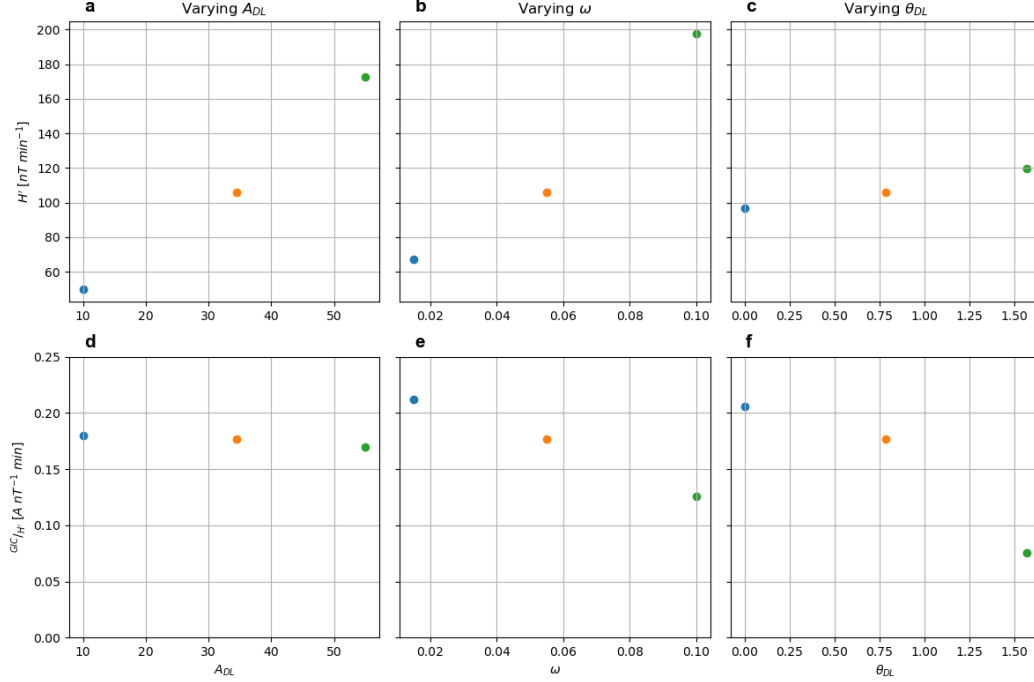
Figure 9. The relationships between the SC model parameters (A_{DL}, ω, and θ_{DL}) and H' (a, b, c), and the gradient of the correlation GIC/H' (d, e, f).

The ω relationship starts similarly, with an increase in ω being linked to an increase in the recorded H' (Figure 9b). However, in this case when we consult the resulting GIC (Figure 9e) we see that the "effectiveness" of the additional H' is reduced as ω increases. In other words there is a larger H' as ω increases (i.e., as the D_L component increases more rapidly), but the resulting current does not increase as quickly as the H': it is not linear or proportionate increase.

We also see that varying θ_{DL} has little impact on the recorded H', small changes are likely due to the interaction between the changing two dimensional D_L, and fixed D_P components of the SC. However, as in Figure 8, we see that the proportionality of the relationship between the maximum H' and modeled GIC changes dramatically. As the D_L component rotates into the East-West orientation the "coupling" between H' and GIC becomes less effective at SDN T2: the same observed maximum H' will be linked to a smaller maximum GIC.

5 Expanding the Synthetic Tests

5.1 Synthetic Model Results Across the South Island of New Zealand

We now expand our consideration from a single transformer (SDN T2) to the southerly portion of the South Island of New Zealand, i.e., that covered by the high resolution MT survey (Ingham et al., 2023). Within this region there are 24 transformers for which we can model the GIC. Figure 10 shows the peak absolute GIC modeled in this part of the network for the base SC event, observed on the 22nd June 2015 (i.e., that shown in orange in Figures 8 and 9). Around 65% of these transformers show small peak GIC, less than 5A, while SDN T2 can be seen on the right at ~ 19 A. It is clear that SDN T2 is
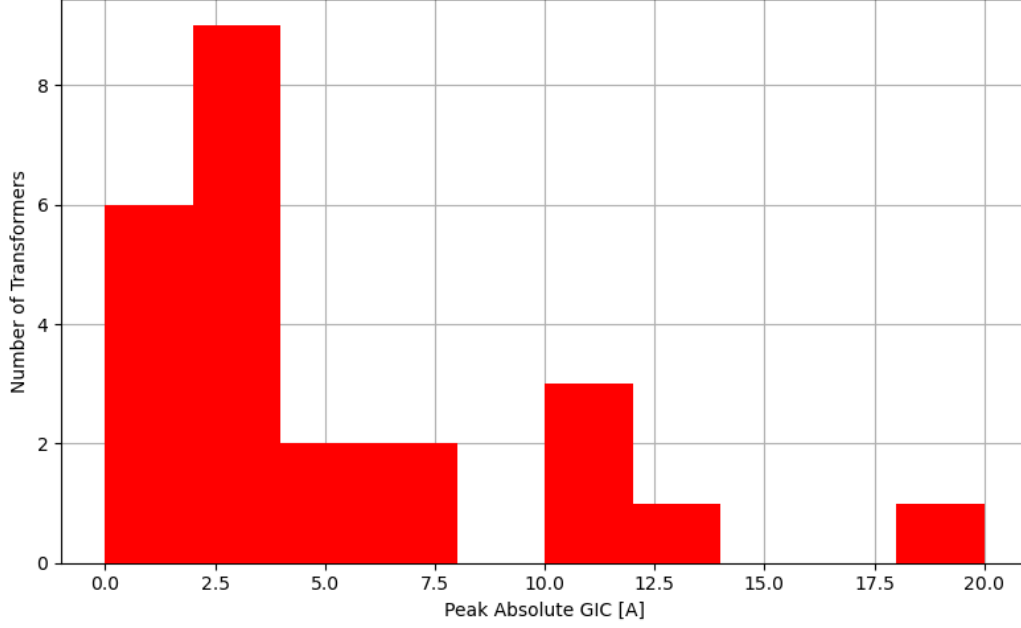
Figure 10. Distribution of peak absolute GIC measured across the South of the South Island of New Zealand for the "baseline" synthetic SC (based on the 22nd June 2015 event), for the 24 locations across the region for which the conductivity model can be used.

the most impacted transformer in this region, as highlighted by previous studies (Mac Manus et al., 2017; Smith, Rodger, et al., 2024).

The distribution in Figure 10 provides us with context, as we now move to discuss the changes in GIC across the network, as a result of changing the fundamental parameters of the SC signature, as in Section 4.1. Figure 11 shows the impact of performing the same three synthetic experiments as above. Each panel shows the distribution of relative GIC observed as a result of increasing (upper panels) or decreasing (lower panels) each parameter, compared to the baseline test. We can see that at almost all locations, reducing the value of A_{DL} reduces the GIC observed (Figure 11a). There is one location for which this is not true (INV T1), but the absolute increase is not huge: 1.3 A to 1.5 A. Increasing A_{DL} increases the peak GIC observed at all locations, by approximately 50% (Figure 11d).

Meanwhile, regarding the tests on the rise time of D_L (ω), we see that - with the values selected - there is a reduced impact on maximum GIC compared to the A_{DL} tests. Reducing ω, i.e., making the step-like change take place over a longer time period, reduces the maximum GIC by up to 50%, while increasing ω increases it correspondingly by up to 50%. It is interesting to note that there is a spectrum of relative change here, where for some locations the change is minimal.

Finally, considering θ_{DL}, in the tests above we showed that these changes largely do not impact H or H', but rather move the D_L change between B_X and B_Y. In this case, largely as expected, we can see both increases and reductions in peak GIC across the network. The magnitude in difference at a single location can be very significant, at some locations the GIC can nearly double with a rotation of D_L of only 45°.
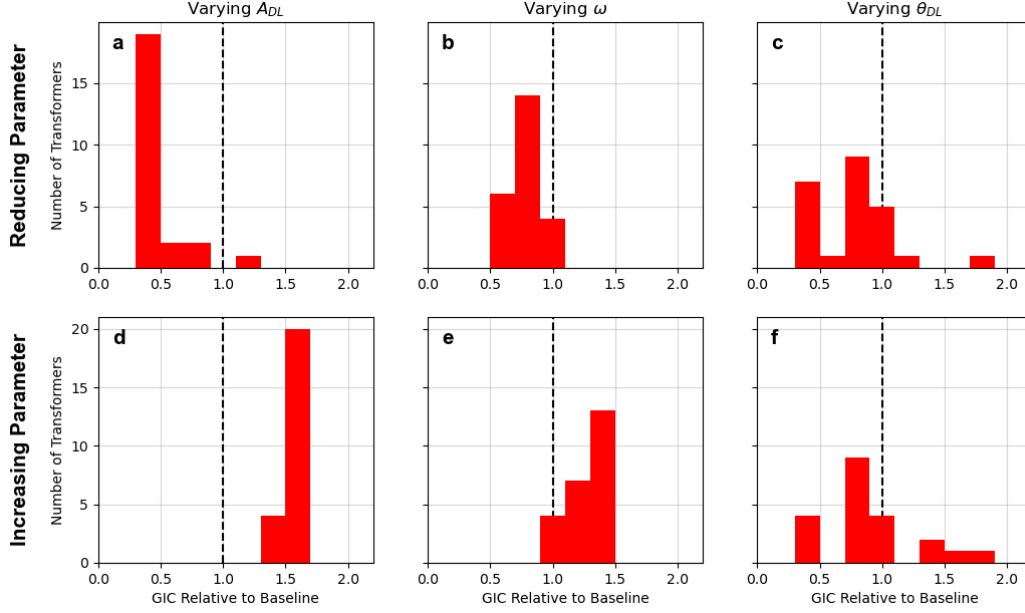
Figure 11. The impact of changing the three key synthetic SC model parameters on the GIC modeled in the Southern South Island of New Zealand. The top row (a, b, c) shows the impact of reducing A_{DL}, ω, and θ_{DL} respectively. The bottom row (d, e, f) shows the impact of increasing A_{DL}, ω, and θ_{DL} respectively. All values are quoted relative to the "base" synthetic test (in turn based on the model fit to the SC on 22nd June 2015).

5.2 Synthetic Model Results on the Induced Geoelectric Field in the United Kingdom

The United Kingdom provides another opportunity to assess the impact of the synthetic SC model tests in a distinct environment, at a comparable geomagnetic latitude to New Zealand, but with very different geology. Enabling this investigation, a recent magnetotelluric survey expanded the coverage within the UK to 70 sites. Beggan et al. (2021) recently showed that such magnetotelluric measurements enable a much better estimation of the induced electric field within the UK, compared to simpler (e.g., thin-sheet) methods due to the UK's complicated geological history and highly variable lithology. For this we rely upon the modelled geoelectric field, as opposed to GICs (c.f. New Zealand, above).

Figure 12 shows the distribution of peak modeled geoelectric field recorded during the "baseline" SC, with the same magnetic signature as was used for the New Zealand tests above. Given the comparable geomagnetic latitude, the use of the same magnetic field signature is assumed to be valid for the purposes of this test. As with the New Zealand tests, we assume no spatial variation of the magnetic signature across the model domain (the United Kingdom). This will not be valid for a real SC (c.f. Smith et al., 2019; Smith, Forsyth, Rae, Rodger, & Freeman, 2021), but nonetheless enables a test where we isolate single changes of SC model parameters across the variable geology of the UK.

The magnetic signature for the "baseline" event (e.g., Figure 7, shown in orange) shows comparable changes in both B_X and B_Y, it is therefore not a surprise that we see considerable (several hundred mV km^{-1}) geoelectric fields in both the North and East (blue and orange in Figure 12). However, around half of the 70 locations report modeled E_X and E_Y of less than $100\,\mathrm{mV\,km^{-1}}$.
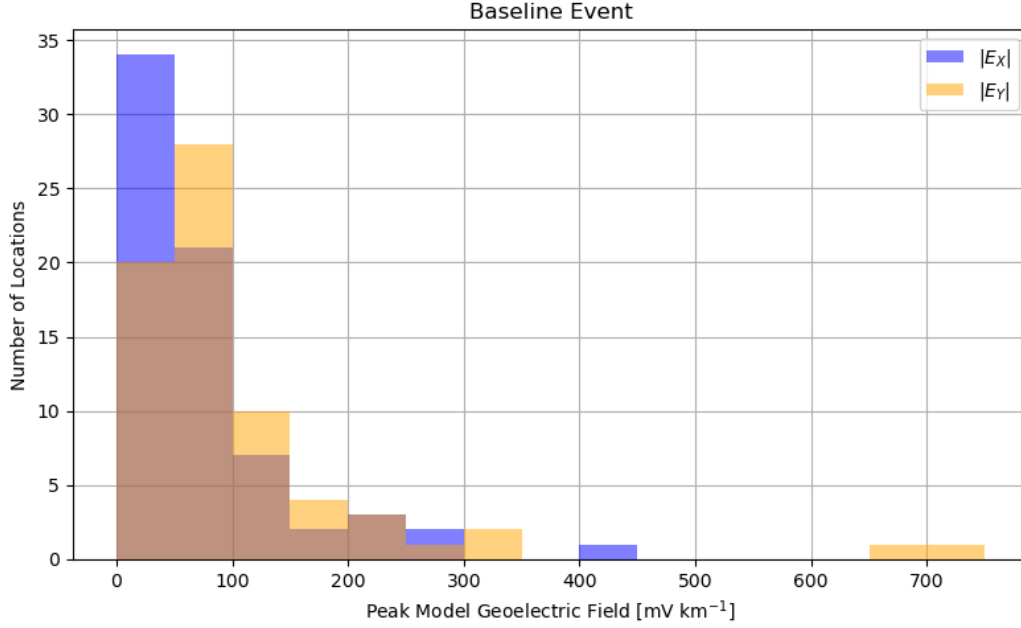
Figure 12. Distribution of peak geoelectric modeled across the United Kingdom for the "baseline" SC (as observed on the 22nd June 2015 at EYR in New Zealand), calculated at 70 sites for which high quality magnetotelluric surveys have been performed. $|E_X|$ and $|E_Y|$ are shown in blue and orange respectively, while the overlap appears brown.

With the context from Figure 12, we now investigate the impact of changing each of the three selected SC model parameters in turn. Figure 13 shows these tests in a similar format to Figure 11. The top row of Figure 13 shows the impact of reducing the three selected parameters, while the bottom row shows the impact of increasing the parameters. We can see that reducing the amplitude of the D_L component (A_{DL}) reduces the modeled geoelectric fields at almost all locations, in both the North and the East directions. This is readily understandable as D_L is equally weighted in both directions. Correspondingly, increasing A_{DL} increases the geoelectric field in both cardinal directions. Interestingly, it seems that for both tests (reducing and increasing A_{DL}) the North-South component of the electric field shows slightly more relative impact, compared to the East-West component, however the distributions do overlap considerably. The median increase/decrease in geoelectric field is approximately 50% for both tests.

Meanwhile, when ω is reduced - the rise time of the D_L component is increased - the corresponding geoelectric field in both cardinal directions is reduced (by a median $\sim 30 - 40\%$), though E_Y shows very little impact in around a third of locations. Increasing ω, i.e., the D_L component has a faster rise, mostly increases the geoelectric field observed at all locations: there is a median increase of around 20%.

Finally, as expected rotating the D_L component differentially impacts the modeled E_X and E_Y. When θ_{DL} is reduced to zero, (Figure 13c), E_X is mostly strongly reduced, while E_Y is mostly increased. The reverse is then true when θ_{DL} is increased to $^{\pi}/_2$ (rotated to the East-West direction): E_Y is reduced, while E_X increases, both by up to a factor of two. Comparing the two tests (Figure 11c and f) it is very interesting to note that the East-West geoelectric field (E_Y) is more persistent than the North-South geoelectric field (E_X). In this case E_Y only reduces by around a factor of two, while E_X can
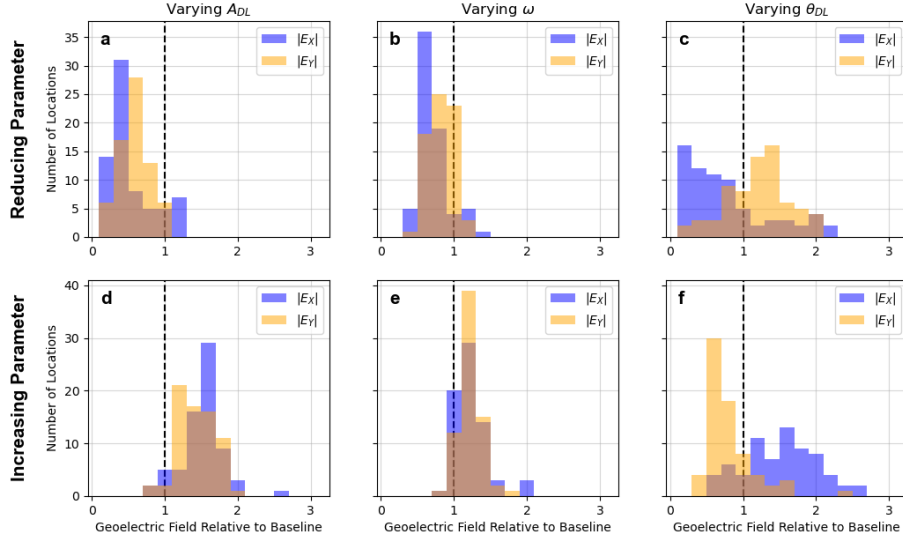
Figure 13. The impact of changing the three key synthetic SC model parameters on the geo-electric field modeled in the United Kingdom. The top row (a, b, c) shows the impact of reducing A_{DL}, ω, and θ_{DL} respectively. The bottom row (d, e, f) shows the impact of increasing A_{DL}, ω, and θ_{DL} respectively. All values are quoted relative to the "base" synthetic test (in turn based on the model fit to the SC on 22nd June 2015 in EYR). As above, $|E_X|$ and $|E_Y|$ are shown in blue and orange respectively, while the overlap appears brown.

in some locations reduce by over 90%. This is due to the complex three dimensional ge-ology of the UK.

6 Discussion

We now discuss our results in the context of the original question: what factors cause an SC to be related to disproportionate GIC? Previous works found that SCs that oc-curred when New Zealand was on the dayside of the Earth were linked to 30% greater GICs on average (e.g., Smith, Forsyth, et al., 2022), for a fixed H'. This could not be explained purely by the changes in the dominant orientation of the SC magnetic signa-ture (e.g., East-West or North-South), and was postulated to be caused by sub-minute resolution details of the sudden commencement geomagnetic signature. Here, we inves-tigate two necessary, but distinct questions: for space weather prediction (a) does 60 s cadence data fully characterize the geomagnetic signature of an SC? (b) Is there intrin-sic variability in the SC signature that can materially impact the GIC observed?

6.1 Data Resolution: Is 60s Cadence Data Sufficient for Characteriz-ing SCs?

From our study, it is strongly suggested that 60 s cadence is not sufficient for cap-turing SC. The magnetic signature of an SC is generally considered to be composed of two main contributions: the D_L and D_P components (Araki, 1994). While both are ul-timately driven by the same physical phenomena, namely the impact of a rapid increase in solar wind dynamic pressure, they are physically distinct and independently vary with magnetic local time, latitude, and season (e.g., Shinbori et al., 2012; Piersanti & Villante,

2016). Both the D_L and D_P perturbations show sub-minute structure, and their observable sum is therefore complex and can only be fully resolved with higher resolution data (e.g., one second resolution), as shown in Figures 3 and 4.

However, simply considering higher resolution data introduces problems with an increased noise contribution, a simple metric such as maximum H' is particularly susceptible to this issue. It is also the case that one second data are only provided to a resolution of $0.1\,\mathrm{nT}$, this needs to be higher (e.g., $0.01\,\mathrm{nT}$). Even were this noise "real", it is unlikely that it would impact the geoelectric field due to the effective bandpass filtering associated with the induction process of the geoelectric field (e.g., Clilverd et al., 2020). If we assume a perfect theoretical correlation, one that is not necessarily expected a priori, an increased noise contribution would act to weaken the correlation. We may see this in Figure 2, where the quality of the correlation between the maximum H' and maximum GIC observed during an SC is reduced upon considering the higher resolution data (e.g., Rodger et al., 2017).

There are several possible solutions to this problem, that would remove the impact of noise while preserving any underlying correlation, for example selecting an intermediate resolution and smoothing the data (e.g., Bower et al., 2024). However, in this study we have chosen to fit an analytical model, based on the physics of the signature (e.g., Araki, 1994), that allows us to gain further valuable insights into the relationship between SCs and GICs. The model also allows us another determination of the maximum H', once the analytical model is fitted to the SCs within this study. We showed that this permitted our maximum H' to better represent the observed magnetic field signature (Figure 4), which in turn increased the correlation between the maximum GIC and H' (Figure 5). This may suggest that the original assumption, that the maximum GIC and a "representative" maximum H' are very well correlated, is a good assumption during SCs (c.f., Rodger et al., 2017; Smith, Forsyth, et al., 2022). This will be dependent upon the local geology, we note that New Zealand's South Island is largely volcanic with a high resistivity.

When we examine the difference between the "naive" maximum H' calculated from $60\,\mathrm{s}$ cadence data, we see that it always underestimates the maximum H' calculated using the analytical model. This underestimation is reflected in the different statistical relationships between the maximum GIC and H' (e.g., Figure 5). With $60\,\mathrm{s}$ data a given maximum H' is inferred to be related to approximately three times larger GICs, solely due to the underestimation of H' by the low resolution data. Similarly, due to the presence of high frequency noise we find that the $1\,\mathrm{s}$ leads to an overestimation of the maximum H'. Statistically in our dataset, this overestimation is a factor of $\sim 25\%$: a given maximum H' is linked to a maximum GIC that is 25% lower.

6.1.1 Variation with Local Time

The figures above were derived from the full statistical dataset, however between different SCs we see that these factors vary within a huge range, $\sim 10 - 80\%$ (Figure 5d). In particular, we note that the $60\,\mathrm{s}$ data tends to underestimate the maximum H' by the greatest factors around dawn and dusk. This may be a result of the D_P component of the SC magnetic signature, linked to the "traveling convection vortices" in the ionosphere (e.g., Friis-Christensen et al., 1988; Clilverd et al., 2021; Madelaire et al., 2022; Oliveira et al., 2024), which form in the morning and afternoon sectors. As shown in Figure 3, the implicit band-pass filtering of the $60\,s$ resolution data does not capture the D_P component of the signature. If the D_L component is small then this will lead to a very large underestimation (e.g., Figure 3b). In particular, we note that the discrepancy appears to be most severe around local dusk (e.g., 18 MLT, Figure 5d), though with such a small number of events we do not consider this to be conclusive.

When comparing the results obtained from the raw 1 s data, it seems that there is a greater tendency to overestimate the maximum H' around local noon (Figure 5d). This could be a result of our small sample size, though it does seem compelling that the two events closest to noon local time both exhibit the largest discrepancy. These events would coincide with the greatest solar illumination, and therefore greatest ionospheric conductivity. However, we do not appear to see a gradual pattern with the remaining 18 events, a tapering off of the effect with local time, for example, perhaps lending credence to the small sample size interpretation.

6.2 Intrinsic Variability: Do Some Types of SC Drive Larger GICs?

Having examined the limitations of conclusions drawn from the 60 s above (in particular with respect to local time), we turn to the second important question: are there intrinsic parameters of an SC that change how effectively it translates to GIC? Figure 5c appeared to show a remnant local time dependence, where SCs that occurred when New Zealand was on the dayside were linked to smaller relative maximum GICs, in contrast to previous studies (c.f., Smith, Forsyth, et al., 2022), when the limitations of the 60 s resolution data are removed. While not definitive, Figure 6 suggested that parameters such as a large ω (i.e., a faster rising D_L component) were linked to smaller GICs for a given maximum H'.

With a small sample size, we did not dwell on a direct examination of the variation of different parameters of the analytical SC model with local time. Instead we turned to synthetic experiments where we test the impact of changing several key parameters in isolation. We focused on three key parameters of the analytical SC model: A_{DL}, ω, and θ_{DL}. We note that increasing A_{DL} and ω naturally increases the maximum H' during the SC, while changing θ_{DL} primarily rotates the magnetic signature between B_X and B_Y, leaving the maximum H' effectively unchanged.

We tested the analytical model, changing each parameter in turn, examining how this impacted the modeled GIC in a transformer in Southern New Zealand. Changing the amplitude of the D_L component (A_{DL}) was found to approximately linearly increase both the maximum H' and maximum GIC in the transformer, such that the relationship between the two was approximately conserved. In contrast, increasing the speed of the rise of the D_L component (ω) increased the maximum H', but the modeled GIC increased at a slower rate. Meanwhile, as expected, changing θ_{DL} changes the link between the maximum H' and maximum GIC as the changing magnetic field will differentially couple to the geology and power network geometry. This test was also performed in the United Kingdom, where we evaluated the geoelectric field at each available MT survey location. We find similar patterns to those observed with the GIC in New Zealand, suggesting the inferences regarding SC properties may be more widely applicable.

6.2.1 Variation with Local Time

Given the discussion above, if ω and θ_{DL} change with local time then that would effectively change the link between maximum H' and resulting GIC. We speculate that ω may vary with local time, for example from the examples in Figure 1, it appears that the SCs on the dayside may "rise" faster, while those on the nightside take longer to reach their peak, i.e., ω may be larger on the dayside. If this were true more generally then this would result in larger H' on the dayside, but a lower effective GIC per unit H' (Figure 9). We note that this will depend on the local geology.

The ionospheric twin-vortices that relate to the D_P component would clearly enforce a local time dependence upon D_P parameters (e.g., Shinbori et al., 2012; Madelaire et al., 2022; Piersanti et al., 2025). The interplay between the combined D_P and D_L components is complex, particularly when a simple parameter such as the maximum

H' is extracted, as illustrated by the H' signatures in Figure 7. A detailed and thorough investigation is therefore required, one that is beyond the scope of the current study. We note that we have exclusively studied the impact of SCs at mid-latitudes, where the D_L and D_P components are both significant, and any potential impact of the equatorial electrojets (e.g., Pulkkinen et al., 2012) is minimal (Curto et al., 2007).

6.3 Impact of Geology

This investigation has been enabled by high spatial resolution magnetotelluric surveys (e.g., Ingham et al., 2023; Huebert et al., 2024). These surveys have enabled the estimation of the impact of short-timescale changes in the magnetic field, beyond that possible with more typical thin-sheet models (e.g., as shown by Pratscher et al., 2024). The correspondence between the model results in the three examples modeled for Figure 1 is excellent, despite a large spatial separation between the magnetic field observations and the monitored transformer (several hundred km).

One of our key findings here is the impact of three dimensional geology on the translation between magnetic field changes, geoelectric field and ultimately GIC. In Figures 12 and 13 we showed that the induced E_Y in the UK is often larger than E_X, despite the synthetic (input) magnetic field changes being approximately evenly split between the two (Figure 7). Further, a significant induced E_Y appears to be present even when the vast majority of the magnetic field change would suggest that it should be negligible (e.g., comparing Figure 13c, f). This highlights the importance of the three-dimensional geology on the induced geoelectric field.

6.4 Space Weather Forecasting Implications

The link between large H' and large GIC has been well established for decades (e.g., Viljanen et al., 2001), with a high correlation observed between the two parameters (Mac Manus et al., 2017; Rodger et al., 2017), particularly during SCs (Smith, Rodger, et al., 2022, 2024). For this reason, recent space weather forecasting models that aim to highlight intervals during which large GICs may be observed have used H' (e.g., Pulkkinen et al., 2013; Pinto et al., 2022; Coughlan et al., 2023), or similar constructs (e.g., R: Smith, Forsyth, Rae, Garton, et al. (2021)), as a proxy target due to the relative abundance of magnetometer data. However, this introduces an additional, intrinsic source of forecast uncertainty, one that is difficult to quantify. Therefore, this study investigates the limitations of relying upon this proxy measurement, when the correspondence may be weaker, and explores potential future avenues for forecasting GICs.

In this study we introduced an analytical model of SCs, with nine free parameters, that describes the initial few minutes of an SC. If these parameters could be determined in advance, for example from properties of the incoming solar wind transient (e.g., Oliveira, 2023), then this would provide a powerful forecasting tool. There is good reason to believe that several of the model parameters should be forecast-able, for example the total change in the D_L component (e.g., A_{DL}) has been related to the square root of the dynamic pressure change for decades (e.g., Siscoe et al., 1968; Su & Konradi, 1975; Russell et al., 1994), as well as the latitude and local time of the location (e.g., Shinbori et al., 2009; Villante & Piersanti, 2009, 2011). Similarly, the value of A_{DP} will depend on the location of the ground magnetometer with respect to the ionospheric current vortices. The changing ionospheric conductivity corresponding to the sunlit/non-sunlit hemispheres of the Earth has also been suggested to determine the ground magnetic field signature of an SC (e.g., Tanaka et al., 2020). Meanwhile, properties such as the impact angle of an interplanetary shock have been noted to be important in determining the GIC that will result, for example through parameters such as θ_{DL} (Villante & Piersanti, 2008; Oliveira et al., 2018; Piersanti et al., 2025). If predicted accurately then the analytical

model presented here would provide a powerful, accurate method of assessing the GIC risk to a given location (e.g., Figure 5).

From this study it is also interesting to note that while larger D_L perturbations (e.g., larger A_{DL}) are linked to larger GICs, the rise time of the D_L component (e.g., larger ω) is also linked to larger GIC. Though a full statistical analysis is beyond the scope of this study, we also consider it likely that larger ω events may be observed when the location is on the dayside of the planet (e.g., Figure 1).

We note that most studies examining the correspondence between H' and GIC have used one minute resolution magnetic field data (e.g., in New Zealand Rodger et al., 2017; Mac Manus et al., 2017), the same cadence of data that space weather forecasting models often target (e.g., Keesee et al., 2020; Smith, Forsyth, Rae, Garton, et al., 2021; Pinto et al., 2022; Coughlan et al., 2023). While the method discussed here will give a more accurate estimate of maximum GIC, during SCs the H' from one minute resolution data still provides a good proxy for GIC during Sudden Commencements, as shown for New Zealand (e.g, Figure 2; Smith, Rodger, et al. (2022, 2024)), so long as the model can sufficiently well forecast such impulsive activity (c.f., Smith, Rae, et al., 2024).

7 Summary and Conclusion

In this study we have investigated why some Sudden Commencements (SCs) appear to be associated with disproportionate GICs, larger or smaller than would be suggested through a relationship with a simple proxy. For example, previous studies have highlighted that SCs that occur when New Zealand is on the dayside of the Earth are linked to 30% greater GICs, even after controlling for several factors (Smith, Rodger, et al., 2022).

First, we tested whether the typical 60 s cadence magnetic field data is capable of capturing the key facets of the geomagnetic signature of an SC at mid-latitudes. We found that 60 s resolution magnetic field data does not include the contributing components of an SC, and that this is particularly a problem at dawn and dusk (e.g., Madelaire et al., 2022; Piersanti et al., 2025). However, simply moving to one second data introduces an additional noise contribution, one that may vary with magnetic local time. We then introduced an analytical model that can accurately describe the key physical components of an SC, namely the D_L and D_P contributions. The use of the well-parameterized SC model revealed a very strong correlation ($r^2 = 0.93$) between the maximum rate of change of the magnetic field (H') and GIC observed during an SC at one location in New Zealand's South Island. Dayside events, particularly those near dusk local times, were most likely to have their magnetic field changes underestimated by 60 s data, partially explaining their tendency to be associated with larger than expected GICs.

Second, we tested whether there is intrinsic variability within SCs that can lead to differential coupling with the induced geoelectric field, and consequently GICs. We used a series of synthetic tests within which we changed a single parameter of the analytical model SC and evaluated its impact on the resulting GIC. We tested the synthetic SC in New Zealand and the United Kingdom through the use of detailed, high spatial resolution magnetotelluric surveys. The first test changed the "size" of the SC, finding that the resulting GIC (and geoelectric fields) scale with this parameter approximately linearly. The second test changed the "rise time" of the SC, how quickly the magnetic field changes during the SC. Within this test we found that a "faster" SC is related to a larger GIC, but this increase is non-linear: the maximum GIC for a given maximum H' reduces. The final test changed the angle of the dominant magnetic field change, with respect to the cardinal directions. The impact of this change varied across a given network/geology, effectively redirecting GIC. However, we found that the three-dimensional geology plays an significant role in moderating this change. Though New Zealand and

	SC Start	SC End
0	2012-10-31 15:38:15	2012-10-31 15:42:45
1	2014-02-07 17:05:00	2014-02-07 17:09:00
2	2014-02-19 03:47:00	2014-02-19 03:51:00
3	2014-02-27 16:49:45	2014-02-27 16:55:30
4	2014-07-14 14:31:30	2014-07-14 14:38:00
5	2014-09-12 15:54:00	2014-09-12 15:57:00
6	2014-11-01 07:05:00	2014-11-01 07:08:00
7	2014-11-10 02:20:00	2014-11-10 02:22:00
8	2015-03-17 04:45:30	2015-03-17 04:48:15
9	2015-03-31 08:32:00	2015-03-31 08:37:00
10	2015-06-21 16:45:00	2015-06-21 16:50:30
11	2015-06-22 05:44:45	2015-06-22 05:48:00
12	2015-06-22 18:33:30	2015-06-22 18:36:00
13	2015-06-24 13:27:00	2015-06-24 13:31:30
14	2015-08-15 08:28:45	2015-08-15 08:33:30
15	2015-09-20 06:03:30	2015-09-20 06:07:30
16	2015-12-19 16:16:30	2015-12-19 16:20:00
17	2015-12-31 00:49:45	2015-12-31 00:57:00
18	2016-03-11 05:32:00	2016-03-11 05:39:00
19	2016-10-12 22:11:00	2016-10-12 22:20:00

the United Kingdom represent very different geologies, they both show the same tendencies, suggesting that these results may be more widely applicable.

These results are of key interest for space weather forecasting. Though H' and GIC do indeed correlate well at a 60 s resolution in New Zealand's South Island (e.g., Mac Manus et al., 2017; Rodger et al., 2017; Smith, Rodger, et al., 2024), we can strengthen this relationship during SCs by modeling the physical components of the SC. Future work should investigate the link between the parameters of the driving solar wind structures (e.g., properties of the interplanetary shock, Oliveira (2023)) and our analytical model. Accurately forecasting the model parameters would enable a robust, accurate estimation of the GIC that may be experienced.

Appendix A SC Event List

This appendix contains a list of the 20 SC events included within this study. The start and end times were empirically determined during the fitting process described above.

Appendix B Testing an Alternative GIC Proxy

For decades the 60 s rate of change of the horizontal geomagnetic field (H') has been the most commonly used proxy for GIC (e.g., Boteler et al., 1998; Viljanen et al., 1999; Pulkkinen et al., 2005), however it is fundamentally limited, as explored in this study. One of the key limitations is that it represents a single, bandpass filtered measurement of the geomagnetic field - a time-series whose frequency content ultimately determines the coupling to the induced geoelectric fields through the geology. Here we demonstrate a test of an alternative GIC proxy (of the geoelectric field) in our study framework: a GIC Index (Marshall et al., 2010, 2011). The benefits of the GIC index are that, as with the magnetic field proxies, no knowledge of the subsurface conductivity is required. This is in contrast to other more complex, but likely more accurate methods (e.g., Piersanti et al., 2019).

Two days (SC ± one day), of one minute data from EYR ($B_X(t)$ and $B_Y(t)$) is used to calculate the GIC index. First, the background (mean magnetic field) is subtracted and a Hamming window is applied. The Fourier transform of the two components of the field are then taken, providing $B_X(f)$ and $B_Y(f)$. The GIC indices are then calculated as follows:

$$GIC_X(t) = |FFT\{B_Y(f)Z(f)\}^{-1}| \tag{B1}$$

$$GIC_Y(t) = |FFT\{B_X(f)Z(f)\}^{-1}| \tag{B2}$$

where $\{FFT\}^{-1}$ is the inverse Fourier transform and $Z(f)$ is a chosen frequency domain filter, in our case:

$$Z(f) = \sqrt{\frac{f}{f_N}}e^{i\frac{\pi}{4}} \tag{B3}$$

as in Marshall et al. (2011), where f_N is the Nyquist frequency. We also calculate a "GIC_H" index as $\sqrt{GIC_X^2 + GIC_Y^2}$. The GIC indices are a proxy for the geoelectric field, and implicitly assume a plane (horizontal) magnetic wave is incident upon a uniformly conducting Earth. We then extract the maximum GIC index at the time of the Sudden Commencements. For context, Marshall et al. (2011) found that GIC indices of the order 50 and 100 correspond to approximate "low" and "moderate" risk levels in terms of documented GIC impact (in Australia). As none of our SCs are associated with known power network impacts in New Zealand we do not expect the values to exceed these benchmarks.

Figure B1 shows the results of correlating the maximum GIC Indices with other derived quantities (proxies and GIC) from our study. The top two rows show the correlation between the maximum GIC Indices and the maximum rate of change of the magnetic field, derived from the two different resolutions considered in this work (top row: 60s, middle row: 1s). The bottom row then shows the correlation between the GIC Indices and the GIC observed at SDN T2, as in Figures 2 and 5.

In the top row, we see that the GIC_Y and GIC_H correlate best with the 60s derived H'. This is interesting, as while both GIC indices and H' (60s) have been used as proxies, and suggests that during impulsive events like SCs both capture the same features. In the second row we find that none of the indices correlate as well ($r^2 < 0.7$) with the 1s derived H'. This could be the result of the greater noise contribution within the 1s H' which was inferred to reduce the correlation in Figure 2. In the final row we see that the maximum GIC_Y index correlates best with the observed maximum GIC at SDN T2 ($r^2 = 0.865$). It is insightful to compare this to the correlations shown in Figure 5, for example we note that this is better than the H' derived from 60s data ($r^2 = 0.845$) and 1s data ($r^2 = 0.65$), but not as good as that derived through the use of our analytical "smoothing" model ($r^2 = 0.928$).

Open Research Section

The results presented in this paper rely on the data collected at the Eyrewell magnetometer station. These data can be found on INTERMAGNET or at GNSScience (2022).

The New Zealand electrical transmission network DC measurements were provided to us by Transpower New Zealand with caveats and restrictions. This includes requirements of permission before all publications and presentations and no ability to provide
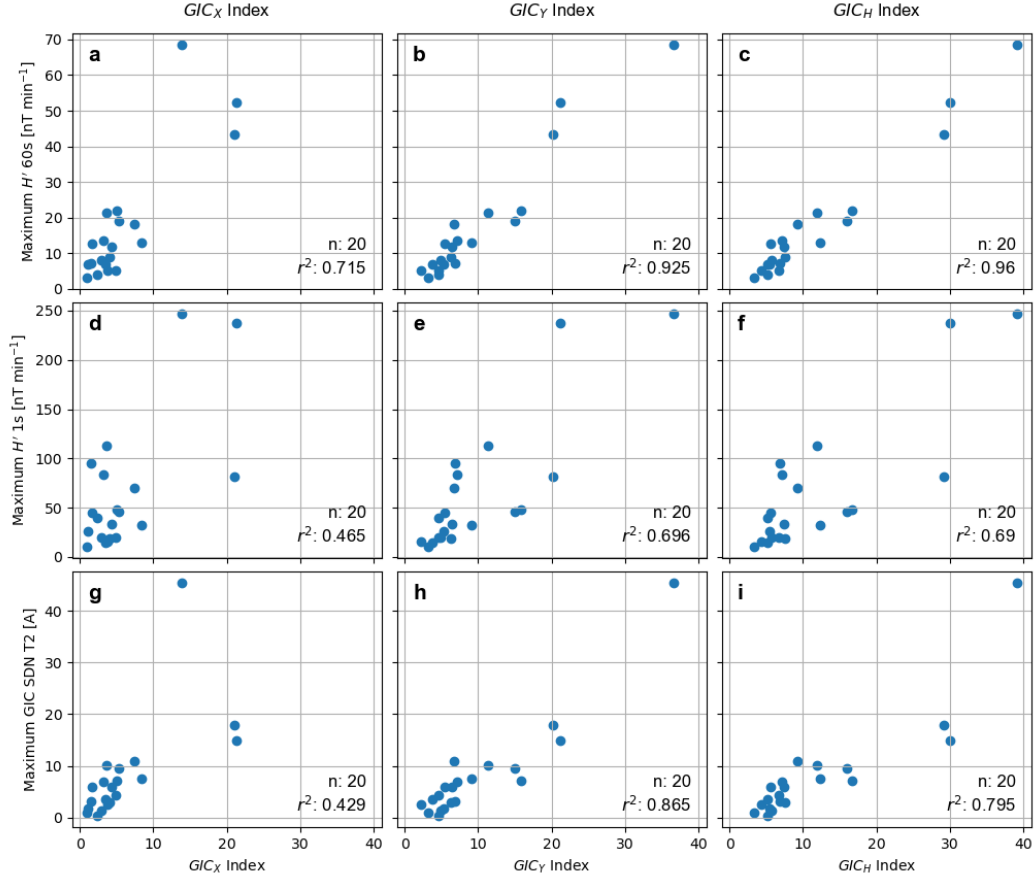
Figure B1. The correlations between the GIC Indices derived through the method outlined above (i.e., Marshall et al., 2011) and several parameters used within this study. The GIC Index is calculated in the X, Y and Horizontal ($\sqrt{GIC_X^2 + GIC_Y^2}$) directions (left, center and right columns, respectively). The parameters of comparison are the maximum H' from the one minute data (top row: a, b, c), one second data (centre row: d, e, f) and the GIC observed at SDN T2 (bottom row: g, h, i).

the observations themselves. Requests for access to these characteristics and the DC measurements need to be made to Transpower New Zealand. At this time, the contact point is M. Dalzell (Michael.Dalzell@transpower.co.nz).

The analysis in this paper was performed using python, including the pandas (McKinney, 2010), NumPy (Van Der Walt et al., 2011), SciPy (Virtanen et al., 2020), emcee (Foreman-Mackey et al., 2012), and Matplotlib (Hunter, 2007) libraries.

Acknowledgments

References

Araki, T.   (1994, jan).   A Physical Model of the Geomagnetic Sudden Commencement.   In M. Engebretson, K. Takahashi, & M. Scholer (Eds.), *Solar wind sources of magnetospheric ultra-low-frequency waves* (p. 183).

Araki, T., Funato, K., Iguchi, T., & Kamei, T.   (1993, may).   Direct detection of solar wind dynamic pressure effect on ground geomagnetic field. *Geophysical Research Letters*, *20*(9), 775–778.   Retrieved from https:// onlinelibrary.wiley.com/doi/full/10.1029/93GL00852https:// onlinelibrary.wiley.com/doi/abs/10.1029/93GL00852https:// agupubs.onlinelibrary.wiley.com/doi/10.1029/93GL00852   doi: 10.1029/93GL00852

Beggan, C. D.   (2015, dec).   Sensitivity of geomagnetically induced currents to varying auroral electrojet and conductivity models. *Earth, Planets and Space*, *67*(1), 24.   Retrieved from http://www.earth-planets-space.com/content/ 67/1/24   doi: 10.1186/s40623-014-0168-9

Beggan, C. D., Richardson, G. S., Baillie, O., Hübert, J., & Thomson, A. W.   (2021).   Geoelectric field measurement, modelling and validation during geomagnetic storms in the UK. *Journal of Space Weather and Space Climate*, *11*, 37.   Retrieved from https://www.swsc-journal.org/articles/swsc/ full{_}html/2021/01/swsc200069/swsc200069.htmlhttps://www.swsc -journal.org/articles/swsc/abs/2021/01/swsc200069/swsc200069.html doi: 10.1051/SWSC/2021022

Blake, S. P., Gallagher, P. T., Campanyà, J., Hogg, C., Beggan, C. D., Thomson, A. W., . . . Bell, D.   (2018).   A Detailed Model of the Irish High Voltage Power Network for Simulating GICs. *Space Weather*, *16*(11), 1770–1783.   Retrieved from https://doi.org/10.1029/2018SW001926   doi: 10.1029/2018SW001926

Boteler, D. H.   (2003).   Geomagnetic hazards to conducting networks. *Natural Hazards*, *28*(2-3), 537–561. Retrieved from http://link.springer.com/10.1023/ A:1022902713136   doi: 10.1023/A:1022902713136

Boteler, D. H., Pirjola, R. J., & Nevanlinna, H.   (1998, jan).   The effects of geomagnetic disturbances on electrical systems at the Earth's surface. *Advances in*

Space Research, *22*(1), 17–27.   Retrieved from `http://linkinghub.elsevier`
`.com/retrieve/pii/S027311779701096X`   doi: 10.1016/S0273-1177(97)01096
-X

Bower, G. E., Imber, S., Milan, S. E., Schillings, A., Fleetham, A. L., & Gjer-
loev, J. W.   (2024, oct).   Location of Geomagnetic Disturbances in Rela-
tion to the Field Aligned Current Boundary.   *Journal of Geophysical Re-*
search: Space Physics, *129*(10), e2024JA033039.   Retrieved from `https://`
`onlinelibrary.wiley.com/doi/full/10.1029/2024JA033039https://`
`onlinelibrary.wiley.com/doi/abs/10.1029/2024JA033039https://`
`agupubs.onlinelibrary.wiley.com/doi/10.1029/2024JA033039`   doi:
10.1029/2024JA033039

Camporeale, E., Cash, M. D., Singer, H. J., Balch, C. C., Huang, Z., & Toth,
G.   (2020, oct).   A gray-box model for a probabilistic estimate of regional
ground magnetic perturbations: Enhancing the NOAA operational Geospace
model with machine learning.   *Journal of Geophysical Research: Space*
Physics.   Retrieved from `https://onlinelibrary.wiley.com/doi/10.1029/`
`2019JA027684`   doi: 10.1029/2019JA027684

Clilverd, M. A., Rodger, C. J., Brundell, J. B., Dalzell, M., Martin, I., Mac Manus,
D. H., & Thomson, N. R.   (2020, oct).   Geomagnetically Induced Currents and
Harmonic Distortion: High Time Resolution Case Studies.   *Space Weather*,
18(10).   Retrieved from `https://onlinelibrary.wiley.com/doi/10.1029/`
`2020SW002594`   doi: 10.1029/2020SW002594

Clilverd, M. A., Rodger, C. J., Freeman, M. P., Brundell, J. B., Mac Manus,
D. H., Dalzell, M., . . . Frame, I.   (2021).   Geomagnetically induced cur-
rents during the 07–08 September 2017 disturbed period: a global perspec-
tive.   *Journal of Space Weather and Space Climate*, *11*, 33.   Retrieved
from `https://www.swsc-journal.org/articles/swsc/full{\_}html/`
`2021/01/swsc200090/swsc200090.htmlhttps://www.swsc-journal.org/`
`articles/swsc/abs/2021/01/swsc200090/swsc200090.html`   doi:
10.1051/SWSC/2021014

Cordell, D., Unsworth, M. J., Lee, B., Hanneson, C., Milling, D. K., & Mann,
I. R.   (2021, oct).   Estimating the Geoelectric Field and Electric Power
Transmission Line Voltage During a Geomagnetic Storm in Alberta, Canada
Using Measured Magnetotelluric Impedance Data: The Influence of Three-
Dimensional Electrical Structures in the Lithosphere.   *Space Weather*, *19*(10),
e2021SW002803.   Retrieved from `https://onlinelibrary.wiley.com/doi/`
`10.1029/2021SW002803`   doi: 10.1029/2021SW002803

Coughlan, M., Keesee, A., Pinto, V., Mukundan, R., Marchezi, J. P., Johnson, J.,
. . . Hampton, D.   (2023, jun).   Probabilistic Forecasting of Ground Mag-
netic Perturbation Spikes at Mid-Latitude Stations.   *Space Weather*, *21*(6),
e2023SW003446.   Retrieved from `https://onlinelibrary.wiley.com/doi/`
`full/10.1029/2023SW003446https://onlinelibrary.wiley.com/doi/abs/`
`10.1029/2023SW003446https://agupubs.onlinelibrary.wiley.com/doi/`
`10.1029/2023SW003446`   doi: 10.1029/2023SW003446

Curto, J. J., Araki, T., & Alberca, L. F.   (2007, nov).   Evolution of the con-
cept of Sudden Storm Commencements and their operative identifica-
tion.   *Earth, Planets and Space*, *59*(11), i–xii.   Retrieved from `http://`
`earth-planets-space.springeropen.com/articles/10.1186/BF03352059`
doi: 10.1186/BF03352059

Dimmock, A. P., Rosenqvist, L., Hall, J. O., Viljanen, A., Yordanova, E., Honkonen,
I., . . . Sjöberg, E. C.   (2019, jun).   The GIC and Geomagnetic Response Over
Fennoscandia to the 7–8 September 2017 Geomagnetic Storm.   *Space Weather*,
17(7), 989–1010.   Retrieved from `https://onlinelibrary.wiley.com/doi/`
`abs/10.1029/2018SW002132`   doi: 10.1029/2018SW002132

Fiori, R. A. D., Boteler, D. H., & Gillies, D. M.   (2014, jan).   Assessment of GIC risk

due to geomagnetic sudden commencements and identification of the current systems responsible. *Space Weather*, *12*(1), 76–91. Retrieved from `http://doi.wiley.com/10.1002/2013SW000967` doi: 10.1002/2013SW000967

Florczak, E., Beggan, C. D., & Whaler, K. A. (2023, mar). The predictive power of magnetospheric models for estimating ground magnetic field variation in the United Kingdom. *Frontiers in Astronomy and Space Sciences*, *10*, 1095971. doi: 10.3389/FSPAS.2023.1095971/BIBTEX

Fogg, A. R., Jackman, C. M., Malone-Leigh, J., Gallagher, P. T., Smith, A. W., Lester, M., ... Waters, J. E. (2023, jul). Extreme Value Analysis of Ground Magnetometer Observations at Valentia Observatory, Ireland. *Space Weather*, *21*(7), e2023SW003565. Retrieved from `https://onlinelibrary.wiley.com/doi/full/10.1029/2023SW003565https://onlinelibrary.wiley.com/doi/abs/10.1029/2023SW003565https://agupubs.onlinelibrary.wiley.com/doi/10.1029/2023SW003565` doi: 10.1029/2023SW003565

Fogg, A. R., Lester, M., Yeoman, T. K., Carter, J. A., Milan, S. E., Sangha, H. K., ... Vines, S. K. (2023, mar). Multi-instrument observations of the effects of a solar wind pressure pulse on the high latitude ionosphere: A detailed case study of a geomagnetic sudden impulse. *Journal of Geophysical Research: Space Physics*, e2022JA031136. Retrieved from `https://onlinelibrary.wiley.com/doi/full/10.1029/2022JA031136https://onlinelibrary.wiley.com/doi/abs/10.1029/2022JA031136https://agupubs.onlinelibrary.wiley.com/doi/10.1029/2022JA031136` doi: 10.1029/2022JA031136

Foreman-Mackey, D., Hogg, D. W., Lang, D., & Goodman, J. (2012, mar). emcee: The MCMC Hammer. *Publications of the Astronomical Society of the Pacific*, *125*(925), 306–312. Retrieved from `http://iopscience.iop.org/article/10.1086/670067http://arxiv.org/abs/1202.3665{\%}0Ahttp://dx.doi.org/10.1086/670067` doi: 10.1086/670067

Friis-Christensen, E., McHenry, M. A., Clauer, C. R., & Vennerstrøm, S. (1988, mar). Ionospheric traveling convection vortices observed near the polar cleft: A triggered response to sudden changes in the solar wind. *Geophysical Research Letters*, *15*(3), 253–256. Retrieved from `http://doi.wiley.com/10.1029/GL015i003p00253` doi: 10.1029/GL015i003p00253

Fujita, S., & Tanaka, T. (2022, dec). Two current systems in the preliminary phase of sudden commencements in the magnetosphere. *Earth, Planets and Space*, *74*(1), 1–17. Retrieved from `https://link.springer.com/articles/10.1186/s40623-022-01624-3https://link.springer.com/article/10.1186/s40623-022-01624-3` doi: 10.1186/S40623-022-01624-3/FIGURES/16

GNSScience. (2022). *Preliminary 1-second and 1-minute data from Eyrewell (EYR) [Data set].* doi: 10.21420/APJY-5050

Grandin, M., Bruus, E., Ledvina, V. E., Partamies, N., Barthelemy, M., Martinis, C., ... Bergstrand, C. (2024, dec). The Gannon Storm: citizen science observations during the geomagnetic superstorm of 10 May 2024. *Geoscience Communication*, *7*(4), 297–316. Retrieved from `https://gc.copernicus.org/articles/7/297/2024/` doi: 10.5194/GC-7-297-2024

Hartinger, M. D., Shi, X., Rodger, C. J., Fujii, I., Rigler, E. J., Kappler, K., ... Petersen, T. (2023, may). Determining ULF Wave Contributions to Geomagnetically Induced Currents: The Important Role of Sampling Rate. *Space Weather*, *21*(5), e2022SW003340. Retrieved from `https://onlinelibrary.wiley.com/doi/full/10.1029/2022SW003340https://onlinelibrary.wiley.com/doi/abs/10.1029/2022SW003340https://agupubs.onlinelibrary.wiley.com/doi/10.1029/2022SW003340` doi: 10.1029/2022SW003340

Hayakawa, H., Ebihara, Y., Mishev, A., Koldobskiy, S., Kusano, K., Bechet, S., ... Miyoshi, Y. (2025, jan). The Solar and Geomagnetic Storms in 2024

May: A Flash Data Report. *The Astrophysical Journal*, *979*(1), 49. Retrieved from `https://iopscience.iop.org/article/10.3847/1538-4357/ad9335https://iopscience.iop.org/article/10.3847/1538-4357/ad9335/meta` doi: 10.3847/1538-4357/AD9335

Heyns, M. J., Lotz, S. I., & Gaunt, C. T. (2021, nov). Geomagnetic Pulsations Driving Geomagnetically Induced Currents. *Space Weather*, *19*(2). Retrieved from `https://onlinelibrary.wiley.com/doi/10.1029/2020SW002557` doi: 10.1029/2020SW002557

Hübert, J., Eaton, E., Beggan, C. D., Montiel-Álvarez, A. M., Kiyan, D., & Hogg, C. (2025). Developing a new ground electric field model for geomagnetically induced currents in Britain based on long-period magnetotelluric data. *Space Weather*, *23*. doi: 10.1029/2025SW004427

Huebert, J., Eaton, E., & Beggan, C. D. (2024). *Developing a new ground electric field model for the UK based on long-period magnetotelluric data for the SWIMMR N4 (SAGE) framework.* Edinburgh, UK. Retrieved from `https://nora.nerc.ac.uk/id/eprint/537960/`

Hunter, J. D. (2007). Matplotlib: A 2D graphics environment [Software]. *Computing in Science and Engineering*, *9*(3), 90–95. Retrieved from `http://ieeexplore.ieee.org/document/4160265/` doi: 10.1109/MCSE.2007.55

Ingham, M., Pratscher, K., Heise, W., Bertrand, E., Kruglyakov, M., & Rodger, C. J. (2023, nov). Influence of Tectonic and Geological Structure on GIC in Southern South Island, New Zealand. *Space Weather*, *21*(11), e2023SW003550. Retrieved from `https://onlinelibrary.wiley.com/doi/full/10.1029/2023SW003550https://onlinelibrary.wiley.com/doi/abs/10.1029/2023SW003550https://agupubs.onlinelibrary.wiley.com/doi/10.1029/2023SW003550` doi: 10.1029/2023SW003550

Keesee, A. M., Pinto, V., Coughlan, M., Lennox, C., Mahmud, M. S., & Connor, H. K. (2020, oct). Comparison of Deep Learning Techniques to Model Connections Between Solar Wind and Ground Magnetic Perturbations. *Frontiers in Astronomy and Space Sciences*, *7*, 72. Retrieved from `https://www.frontiersin.org/article/10.3389/fspas.2020.550874/full` doi: 10.3389/fspas.2020.550874

Kikuchi, T., Araki, T., Hashimoto, K. K., Ebihara, Y., Tanaka, T., Nishimura, Y., ... Kadokura, A. (2022, may). Instantaneous Achievement of the Hall and Pedersen–Cowling Current Circuits in Northern and Southern Hemispheres During the Geomagnetic Sudden Commencement on 12 May 2021. *Frontiers in Astronomy and Space Sciences*, *9*, 879314. Retrieved from `www.frontiersin.org` doi: 10.3389/FSPAS.2022.879314/BIBTEX

Kokubun, S. (1983, dec). Characteristics of storm sudden commencement at geostationary orbit. *Journal of Geophysical Research*, *88*(A12), 10025. Retrieved from `http://doi.wiley.com/10.1029/JA088iA12p10025` doi: 10.1029/JA088iA12p10025

Lam, M. M., & Rodger, A. S. (2001, jul). A case study test of Araki's physical model of geomagnetic sudden commencement. *Journal of Geophysical Research: Space Physics*, *106*(A7), 13135–13144. Retrieved from `http://doi.wiley.com/10.1029/2000JA900134` doi: 10.1029/2000JA900134

Mac Manus, D. H., Rodger, C. J., Dalzell, M., Thomson, A. W., Clilverd, M. A., Petersen, T., ... Divett, T. (2017, aug). Long-term geomagnetically induced current observations in New Zealand: Earth return corrections and geomagnetic field driver. *Space Weather*, *15*(8), 1020–1038. Retrieved from `http://doi.wiley.com/10.1002/2017SW001635` doi: 10.1002/2017SW001635

Mac Manus, D. H., Rodger, C. J., Ingham, M., Clilverd, M. A., Dalzell, M., Divett, T., ... Petersen, T. (2022). Geomagnetically Induced Current Model in New Zealand Across Multiple Disturbances: Validation and Extension to Non-Monitored Transformers. *Space Weather*, *20*(2). doi: 10.1029/2021SW002955

Mac Manus, D. H., Rodger, C. J., Renton, A., Ronald, J., Harper, D., Taylor, C., ... Clilverd, M. A. (2023, nov). Geomagnetically Induced Current Mitigation in New Zealand: Operational Mitigation Method Development With Industry Input. *Space Weather*, *21*(11), e2023SW003533. Retrieved from `https:// onlinelibrary.wiley.com/doi/full/10.1029/2023SW003533https:// onlinelibrary.wiley.com/doi/abs/10.1029/2023SW003533https:// agupubs.onlinelibrary.wiley.com/doi/10.1029/2023SW003533` doi: 10.1029/2023SW003533

Madelaire, M., Laundal, K. M., Reistad, J. P., Hatch, S. M., & Ohma, A. (2022, aug). Transient high latitude geomagnetic response to rapid increases in solar wind dynamic pressure. *Frontiers in Astronomy and Space Sciences*, *9*, 953954. doi: 10.3389/FSPAS.2022.953954/BIBTEX

Madsen, F. D., Beggan, C. D., & Whaler, K. A. (2022, oct). Forecasting changes of the magnetic field in the United Kingdom from L1 Lagrange solar wind measurements. *Frontiers in Physics*, *0*, 1091. Retrieved from `https:// www.frontiersin.org/articles/10.3389/fphy.2022.1017781/full` doi: 10.3389/FPHY.2022.1017781

Marshall, R. A., Dalzell, M., Waters, C. L., Goldthorpe, P., & Smith, E. A. (2012, aug). Geomagnetically induced currents in the New Zealand power network. *Space Weather*, *10*(8), n/a–n/a. Retrieved from `http://doi.wiley.com/10 .1029/2012SW000806` doi: 10.1029/2012SW000806

Marshall, R. A., Smith, E. A., Francis, M. J., Waters, C. L., & Sciffer, M. D. (2011, oct). A preliminary risk assessment of the Australian region power network to space weather. *Space Weather*, *9*(10). Retrieved from `https:// onlinelibrary.wiley.com/doi/full/10.1029/2011SW000685https:// onlinelibrary.wiley.com/doi/abs/10.1029/2011SW000685https:// agupubs.onlinelibrary.wiley.com/doi/10.1029/2011SW000685` doi: 10.1029/2011SW000685

Marshall, R. A., Waters, C. L., & Sciffer, M. D. (2010, may). Spectral analysis of pipe-to-soil potentials with variations of the Earth's magnetic field in the Australian region. *Space Weather*, *8*(5). Retrieved from `https:// onlinelibrary.wiley.com/doi/full/10.1029/2009SW000553https:// onlinelibrary.wiley.com/doi/abs/10.1029/2009SW000553https:// agupubs.onlinelibrary.wiley.com/doi/10.1029/2009SW000553` doi: 10.1029/2009SW000553

McKinney, W. (2010). *Data Structures for Statistical Computing in Python [Software]*. Retrieved from `http://conference.scipy.org/proceedings/ scipy2010/mckinney.html`

Moretto, T., Hesse, M., Yahnin, A., Ieda, A., Murr, D., & Watermann, J. F. (2002). Magnetospheric signature of an ionospheric traveling convection vortex event. Retrieved from `https://www.researchgate.net/profile/ Alexander-Yahnin/publication/236490348{\_}Magnetospheric{\ _}signature{\_}of{\_}an{\_}ionospheric{\_}traveling{\_}convection{\ _}vortex{\_}event/links/00b7d517faa16655c5000000/Magnetospheric -signature-of-an-ionospheric-traveling-convection-vortex-` doi: 10.1029/2001JA000049

Oliveira, D. M. (2023, sep). Interplanetary shock data base. *Frontiers in Astronomy and Space Sciences*, *10*, 1240323. Retrieved from `https:// www.frontiersin.org/articles/10.3389/fspas.2023.1240323/full` doi: 10.3389/FSPAS.2023.1240323

Oliveira, D. M., Arel, D., Raeder, J., Zesta, E., Ngwira, C. M., Carter, B. A., ... Gjerloev, J. W. (2018, jun). Geomagnetically Induced Currents Caused by Interplanetary Shocks With Different Impact Angles and Speeds. *Space Weather*, *16*(6), 636–647. Retrieved from `http://doi.wiley.com/10.1029/ 2018SW001880` doi: 10.1029/2018SW001880

Oliveira, D. M., Zesta, E., & Vidal-Luengo, S.   (2024, jul).   First direct observations of interplanetary shock impact angle effects on actual geomagnetically induced currents: The case of the Finnish natural gas pipeline system. *Frontiers in Astronomy and Space Sciences*, *11*, 1392697.   Retrieved from `https://dennyoliveira`.   doi: 10.3389/FSPAS.2024.1392697/PDF

Oughton, E. J., Hapgood, M., Richardson, G. S., Beggan, C. D., Thomson, A. W., Gibbs, M., . . . Horne, R. B. (2019, may). A Risk Assessment Framework for the Socioeconomic Impacts of Electricity Transmission Infrastructure Failure Due to Space Weather: An Application to the United Kingdom. *Risk Analysis*, *39*(5), 1022–1043.   Retrieved from `https://onlinelibrary.wiley.com/doi/abs/10.1111/risa.13229` doi: 10.1111/risa.13229

Piersanti, M., Di Matteo, S., Carter, B. A., Currie, J., & D'Angelo, G.   (2019, aug). Geoelectric Field Evaluation During the September 2017 Geomagnetic Storm: MA.I.GIC. Model. *Space Weather*, *17*(8), 1241–1256. Retrieved from `https://onlinelibrary.wiley.com/doi/full/10.1029/2019SW002202https://onlinelibrary.wiley.com/doi/abs/10.1029/2019SW002202https://agupubs.onlinelibrary.wiley.com/doi/10.1029/2019SW002202`   doi: 10.1029/2019SW002202

Piersanti, M., Oliveira, D. M., D'Angelo, G., Diego, P., Napoletano, G., & Zesta, E.   (2025, feb).   On the Geoelectric Field Response to the SSC of the May 2024 Super Storm Over Europe.   *Space Weather*, *23*(2), e2024SW004191. Retrieved from `https://onlinelibrary.wiley.com/doi/full/10.1029/2024SW004191https://onlinelibrary.wiley.com/doi/abs/10.1029/2024SW004191https://agupubs.onlinelibrary.wiley.com/doi/10.1029/2024SW004191` doi: 10.1029/2024SW004191

Piersanti, M., & Villante, U.   (2016, jul).   On the discrimination between magnetospheric and ionospheric contributions on the ground manifestation of sudden impulses. *Journal of Geophysical Research: Space Physics*, *121*(7), 6674–6691. Retrieved from `https://onlinelibrary.wiley.com/doi/full/10.1002/2015JA021666https://onlinelibrary.wiley.com/doi/abs/10.1002/2015JA021666https://agupubs.onlinelibrary.wiley.com/doi/10.1002/2015JA021666` doi: 10.1002/2015JA021666

Pinto, V. A., Keesee, A. M., Coughlan, M., Mukundan, R., Johnson, J. W., Ngwira, C. M., & Connor, H. K.   (2022, may).   Revisiting the Ground Magnetic Field Perturbations Challenge: A Machine Learning Perspective. *Frontiers in Astronomy and Space Sciences*, *9*, 123.   Retrieved from `https://www.frontiersin.org/articles/10.3389/fspas.2022.869740/full`   doi: 10.3389/fspas.2022.869740

Pratscher, K. M., Ingham, M., Manus, D. H. M., Kruglyakov, M., Heise, W., Rodger, C. J., . . . Brundell, J.   (2024, jul).   Modeling GIC in the Southern South Island of Aotearoa New Zealand Using Magnetotelluric Data. *Space Weather*, *22*(7), e2024SW003907.   Retrieved from `https://onlinelibrary.wiley.com/doi/full/10.1029/2024SW003907https://onlinelibrary.wiley.com/doi/abs/10.1029/2024SW003907https://agupubs.onlinelibrary.wiley.com/doi/10.1029/2024SW003907`   doi: 10.1029/2024SW003907

Pulkkinen, A., Bernabeu, E., Eichner, J., Beggan, C., & Thomson, A. W.   (2012, apr). Generation of 100-year geomagnetically induced current scenarios. *Space Weather*, *10*(4), 4003.   Retrieved from `https://onlinelibrary.wiley.com/doi/full/10.1029/2011SW000750https://onlinelibrary.wiley.com/doi/abs/10.1029/2011SW000750https://agupubs.onlinelibrary.wiley.com/doi/10.1029/2011SW000750` doi: 10.1029/2011SW000750

Pulkkinen, A., Lindahl, S., Viljanen, A., & Pirjola, R.   (2005, aug).   Geomagnetic storm of 29-31 October 2003: Geomagnetically induced currents and their relation to problems in the Swedish high-voltage power transmission system. *Space*

Weather, *3*(8), n/a–n/a. Retrieved from http://doi.wiley.com/10.1029/2004SW000123 doi: 10.1029/2004SW000123

Pulkkinen, A., Rastätter, L., Kuznetsova, M., Singer, H., Balch, C., Weimer, D., . . . Weigel, R. (2013, jun). Community-wide validation of geospace model ground magnetic field perturbation predictions to support model transition to operations. *Space Weather*, *11*(6), 369–385. Retrieved from http://doi.wiley.com/10.1002/swe.20056 doi: 10.1002/swe.20056

Rodger, C. J., Mac Manus, D. H., Dalzell, M., Thomson, A. W. P., Clarke, E., Petersen, T., . . . Divett, T. (2017, nov). Long-Term Geomagnetically Induced Current Observations From New Zealand: Peak Current Estimates for Extreme Geomagnetic Storms. *Space Weather*, *15*(11), 1447–1460. Retrieved from http://doi.wiley.com/10.1002/2017SW001691 doi: 10.1002/2017SW001691

Rogers, N. C., Wild, J. A., Eastoe, E. F., Gjerloev, J. W., & Thomson, A. W. P. (2020, feb). A global climatological model of extreme geomagnetic field fluctuations. *Journal of Space Weather and Space Climate*, *10*, 5. Retrieved from https://www.swsc-journal.org/10.1051/swsc/2020008 doi: 10.1051/swsc/2020008

Russell, C. T., Ginskey, M., Petrinec, S., & Le, G. (1992, jun). The effect of solar wind dynamic pressure changes on low and mid-latitude magnetic records. *Geophysical Research Letters*, *19*(12), 1227–1230. Retrieved from http://doi.wiley.com/10.1029/92GL01161 doi: 10.1029/92GL01161

Russell, C. T., Ginskey, M., & Petrinec, S. M. (1994, jul). Sudden impulses at low latitude stations: Steady state response for southward interplanetary magnetic field. *Journal of Geophysical Research*, *99*(A7), 13403. Retrieved from http://doi.wiley.com/10.1029/94JA00549 doi: 10.1029/94JA00549

Shinbori, A., Tsuji, Y., Kikuchi, T., Araki, T., Ikeda, A., Uozumi, T., . . . Yumoto, K. (2012). Magnetic local time and latitude dependence of amplitude of the main impulse (MI) of geomagnetic sudden commencements and its seasonal variation. *Journal of Geophysical Research: Space Physics*, *117*(8), 8322. Retrieved from http://cdaweb.gsfc. doi: 10.1029/2012JA018006

Shinbori, A., Tsuji, Y., Kikuchi, T., Araki, T., & Watari, S. (2009, apr). Magnetic latitude and local time dependence of the amplitude of geomagnetic sudden commencements. *Journal of Geophysical Research: Space Physics*, *114*(A4), 4217. Retrieved from https://onlinelibrary.wiley.com/doi/full/10.1029/2008JA013871https://onlinelibrary.wiley.com/doi/abs/10.1029/2008JA013871https://agupubs.onlinelibrary.wiley.com/doi/10.1029/2008JA013871 doi: 10.1029/2008JA013871

Siscoe, G. L., Formisano, V., & Lazarus, A. J. (1968, aug). Relation between geomagnetic sudden impulses and solar wind pressure changes—An experimental investigation. *Journal of Geophysical Research*, *73*(15), 4869–4874. Retrieved from https://onlinelibrary.wiley.com/doi/full/10.1029/JA073i015p04869https://onlinelibrary.wiley.com/doi/abs/10.1029/JA073i015p04869https://agupubs.onlinelibrary.wiley.com/doi/10.1029/JA073i015p04869 doi: 10.1029/JA073I015P04869

Smith, A. W., Forsyth, C., Rae, I. J., Garton, T. M., Bloch, T., Jackman, C. M., & Bakrania, M. (2021, aug). Forecasting the Probability of Large Rates of Change of the Geomagnetic Field in the UK: Timescales, Horizons and Thresholds. *Space Weather*, e2021SW002788. Retrieved from https://onlinelibrary.wiley.com/doi/10.1029/2021SW002788 doi: 10.1029/2021SW002788

Smith, A. W., Forsyth, C., Rae, I. J., Garton, T. M., Jackman, C. M., Bakrania, M., . . . Johnson, J. M. (2022, jul). On the Considerations of Using Near Real Time Data for Space Weather Hazard Forecasting. *Space Weather*, *20*(7), e2022SW003098. Retrieved from https://onlinelibrary.wiley.com/doi/

full/10.1029/2022SW003098https://onlinelibrary.wiley.com/doi/abs/
10.1029/2022SW003098https://agupubs.onlinelibrary.wiley.com/doi/
10.1029/2022SW003098 doi: 10.1029/2022SW003098

Smith, A. W., Forsyth, C., Rae, J., Rodger, C. J., & Freeman, M. P.   (2021, jun).   The Impact of Sudden Commencements on Ground Magnetic Field Variability: Immediate and Delayed Consequences.   *Space Weather*, *19*(7), e2021SW002764.   Retrieved from https://onlinelibrary.wiley.com/doi/10.1029/2021SW002764 doi: 10.1029/2021SW002764

Smith, A. W., Freeman, M. P., Rae, I. J., & Forsyth, C. (2019, nov). The Influence of Sudden Commencements on the Rate of Change of the Surface Horizontal Magnetic Field in the United Kingdom.   *Space Weather*, *17*(11), 1605–1617.   Retrieved from https://onlinelibrary.wiley.com/doi/abs/10.1029/2019SW002281 doi: 10.1029/2019SW002281

Smith, A. W., Jackman, C. M., Frohmaier, C. M., Coxon, J. C., Slavin, J. A., & Fear, R. C. (2018, dec). Evaluating Single-Spacecraft Observations of Planetary Magnetotails With Simple Monte Carlo Simulations: 1. Spatial Distributions of the Neutral Line.   *Journal of Geophysical Research: Space Physics*, *123*(12), 10,109–10,123. Retrieved from https://onlinelibrary.wiley.com/doi/abs/10.1029/2018JA025958 doi: 10.1029/2018JA025958

Smith, A. W., Rae, I. J., Forsyth, C., Coxon, J. C., Walach, M.-T., Lao, C. J., ... Bentley, S.   (2024, nov).   Space Weather Forecasts of Ground Level Space Weather in the UK: Evaluating Performance and Limitations.   *Space Weather*, *22*(11), e2024SW003973.   Retrieved from https://onlinelibrary.wiley.com/doi/full/10.1029/2024SW003973https://onlinelibrary.wiley.com/doi/abs/10.1029/2024SW003973https://agupubs.onlinelibrary.wiley.com/doi/10.1029/2024SW003973   doi: 10.1029/2024SW003973

Smith, A. W., Rodger, C. J., Mac Manus, D. H., Forsyth, C., Rae, I. J., Freeman, M. P., ... Dalzell, M.   (2022, aug).   The Correspondence Between Sudden Commencements and Geomagnetically Induced Currents: Insights From New Zealand. *Space Weather*, *20*(8), e2021SW002983. Retrieved from https://onlinelibrary.wiley.com/doi/full/10.1029/2021SW002983https://onlinelibrary.wiley.com/doi/abs/10.1029/2021SW002983https://agupubs.onlinelibrary.wiley.com/doi/10.1029/2021SW002983   doi: 10.1029/2021SW002983

Smith, A. W., Rodger, C. J., Mac Manus, D. H., Rae, I. J., Fogg, A. R., Forsyth, C., ... Dalzell, M.   (2024, jan).   Sudden Commencements and Geomagnetically Induced Currents in New Zealand: Correlations and Dependance. *Space Weather*, *22*(1), e2023SW003731.   Retrieved from https://onlinelibrary.wiley.com/doi/full/10.1029/2023SW003731https://onlinelibrary.wiley.com/doi/abs/10.1029/2023SW003731https://agupubs.onlinelibrary.wiley.com/doi/10.1029/2023SW003731   doi: 10.1029/2023SW003731

Su, S.-Y., & Konradi, A.   (1975, jan).   Magnetic field depression at the Earth's surface calculated from the relationship between the size of the magnetosphere and the Dst values.   *Journal of Geophysical Research*, *80*(1), 195–199.   Retrieved from https://onlinelibrary.wiley.com/doi/full/10.1029/JA080i001p00195https://onlinelibrary.wiley.com/doi/abs/10.1029/JA080i001p00195https://agupubs.onlinelibrary.wiley.com/doi/10.1029/JA080i001p00195 doi: 10.1029/JA080I001P00195

Tanaka, T., Ebihara, Y., Watanabe, M., Den, M., Fujita, S., Kikuchi, T., ... Kataoka, R. (2020, feb). Reproduction of Ground Magnetic Variations During the SC and the Substorm From the Global Simulation and Biot-Savart's Law. *Journal of Geophysical Research: Space Physics*, *125*(2), e2019JA027172. Retrieved from https://onlinelibrary.wiley.com/doi/full/10.1029/

2019JA027172https://onlinelibrary.wiley.com/doi/abs/10.1029/
2019JA027172https://agupubs.onlinelibrary.wiley.com/doi/10.1029/
2019JA027172 doi: 10.1029/2019JA027172

Tanskanen, E. I., Viljanen, A., Pulkkinen, T. I., Pirjola, R., Hakkinen, L., Pulkki-
nen, A., & Amm, O. (2001, jul). At substorm onset 40\% of AL comes from
underground. *Journal of Geophysical Research: Space Physics*, *106*(A7),
13119–13134. Retrieved from http://doi.wiley.com/10.1029/2000JA900135
doi: 10.1029/2000JA900135

Thomson, A. W., Dawson, E. B., & Reay, S. J. (2011, oct). Quantifying extreme be-
havior in geomagnetic activity. *Space Weather*, *9*(10). Retrieved from http://
doi.wiley.com/10.1029/2011SW000696 doi: 10.1029/2011SW000696

Upendran, V., Tigas, P., Ferdousi, B., Bloch, T., Cheung, M. C. M., Ganju, S.,
... Gal, Y. (2022, may). Global geomagnetic perturbation forecasting
using Deep Learning. *Space Weather*, e2022SW003045. Retrieved from
https://onlinelibrary.wiley.com/doi/10.1029/2022SW003045 doi:
10.1029/2022SW003045

Van Der Walt, S., Colbert, S. C., & Varoquaux, G. (2011, mar). The NumPy array:
A structure for efficient numerical computation [Software]. *Computing in Sci-
ence and Engineering*, *13*(2), 22–30. Retrieved from http://ieeexplore.ieee
.org/document/5725236/ doi: 10.1109/MCSE.2011.37

Viljanen, A., Amm, O., & Pirjola, R. (1999, dec). Modeling geomagnetically in-
duced currents during different ionospheric situations. *Journal of Geophysical
Research: Space Physics*, *104*(A12), 28059–28071. Retrieved from http://doi
.wiley.com/10.1029/1999JA900337 doi: 10.1029/1999JA900337

Viljanen, A., Nevanlinna, H., Pajunpää, K., & Pulkkinen, A. (2001). Time deriva-
tive of the horizontal geomagnetic field as an activity indicator. *Annales Geo-
physicae*, *19*(9), 1107–1118. Retrieved from http://www.ann-geophys.net/
19/1107/2001/ doi: 10.5194/angeo-19-1107-2001

Villante, U., & Piersanti, M. (2008, aug). An analysis of sudden impulses at
geosynchronous orbit. *Journal of Geophysical Research: Space Physics*,
113(A8), 8213. Retrieved from https://onlinelibrary.wiley.com/doi/
full/10.1029/2008JA013028https://onlinelibrary.wiley.com/doi/abs/
10.1029/2008JA013028https://agupubs.onlinelibrary.wiley.com/doi/
10.1029/2008JA013028 doi: 10.1029/2008JA013028

Villante, U., & Piersanti, M. (2009, jun). Analysis of geomagnetic sudden im-
pulses at low latitudes. *Journal of Geophysical Research: Space Physics*,
114(A6), 6209. Retrieved from https://onlinelibrary.wiley.com/doi/
full/10.1029/2008JA013920https://onlinelibrary.wiley.com/doi/abs/
10.1029/2008JA013920https://agupubs.onlinelibrary.wiley.com/doi/
10.1029/2008JA013920 doi: 10.1029/2008JA013920

Villante, U., & Piersanti, M. (2011, jan). Sudden impulses at geosynchronous orbit
and at ground. *Journal of Atmospheric and Solar-Terrestrial Physics*, *73*(1),
61–76. doi: 10.1016/J.JASTP.2010.01.008

Virtanen, P., Gommers, R., Oliphant, T. E., Haberland, M., Reddy, T., Cournapeau,
D., ... Contributors, S. . . (2020). SciPy 1.0: Fundamental Algorithms for
Scientific Computing in Python [Software]. *Nature Methods*, *17*, 261–272. doi:
https://doi.org/10.1038/s41592-019-0686-2

Wang, T., Fletcher, D., Parry, M., Rodger, C. J., Smith, A. W., & Petersen, T.
(2025, jul). Better Forecasting of Extreme Geomagnetic Storms Using Non-
Stationary Statistical Models. *Space Weather*, *23*(7), e2025SW004404. Re-
trieved from https://onlinelibrary.wiley.com/doi/full/10.1029/
2025SW004404https://onlinelibrary.wiley.com/doi/abs/10.1029/
2025SW004404https://agupubs.onlinelibrary.wiley.com/doi/10.1029/
2025SW004404 doi: 10.1029/2025SW004404

Wintoft, P., Wik, M., & Viljanen, A. (2015, mar). Solar wind driven empirical

forecast models of the time derivative of the ground magnetic field.   *Journal of Space Weather and Space Climate*, *5*, A7.   Retrieved from `http://www.swsc-journal.org/10.1051/swsc/2015008`   doi: 10.1051/swsc/2015008

Figure 1.
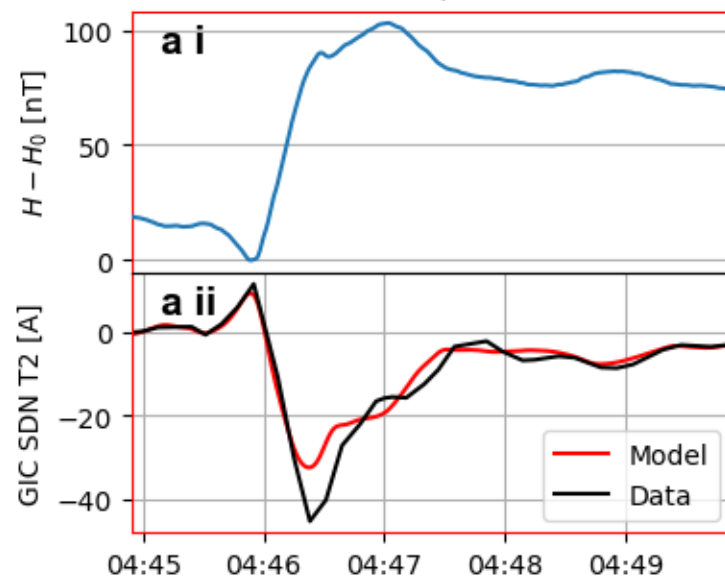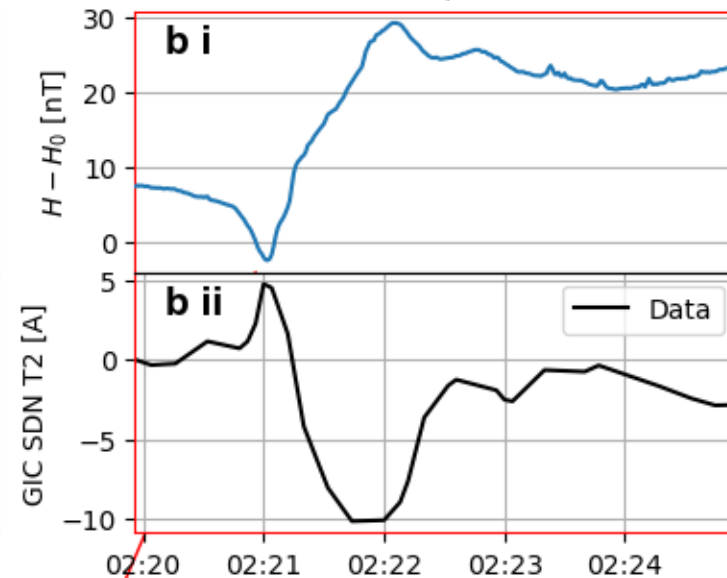
Figure panels:

17-03-2015; MLT: 16.7
a i — $H - H_0$ [nT]
a ii — GIC SDN T2 [A] (Model, Data)

10-11-2014; MLT: 14.6
b i — $H - H_0$ [nT]
b ii — GIC SDN T2 [A] (Data)

22-06-2015; MLT: 17.8
c i — $H - H_0$ [nT]
c ii — GIC SDN T2 [A] (Data)

22-06-2015; MLT: 6.8
d i — $H - H_0$ [nT]
d ii — GIC SDN T2 [A] (Model, Data)

15-08-2015; MLT: 20.4
e i — $H - H_0$ [nT]
e ii — GIC SDN T2 [A] (Data)

12-09-2014; MLT: 4.1
f i — $H - H_0$ [nT]
f ii — GIC SDN T2 [A] (Model, Data)

Center diagram labels: 12 UT, 6 UT, 18 UT, 24 UT

Figure 2.

a 60s Resolution $|H'|$ Data

b 1s Resolution $|H'|$ Data

GIC SDN T2 [A]

H' [nT min^{-1}]

Panel a:
n: 20
m: 0.504 +- 0.037
c: 0.0
r^2: 0.846

Panel b:
n: 20
m: 0.123 +- 0.014
c: 0.0
r^2: 0.65
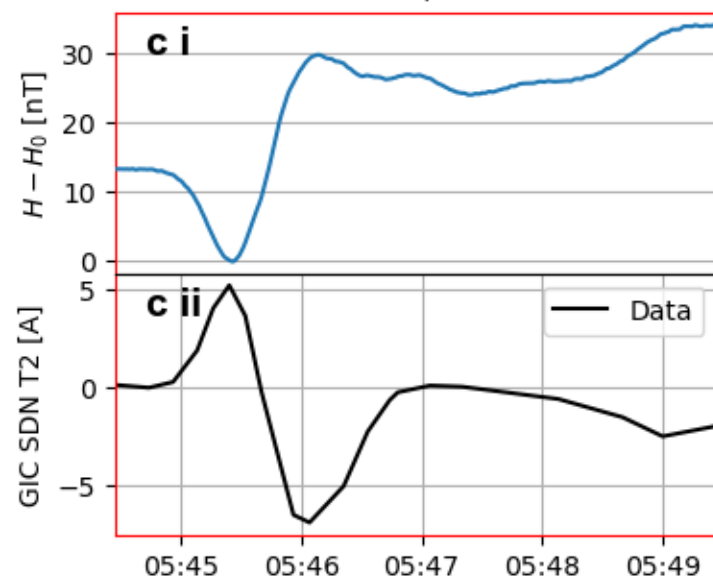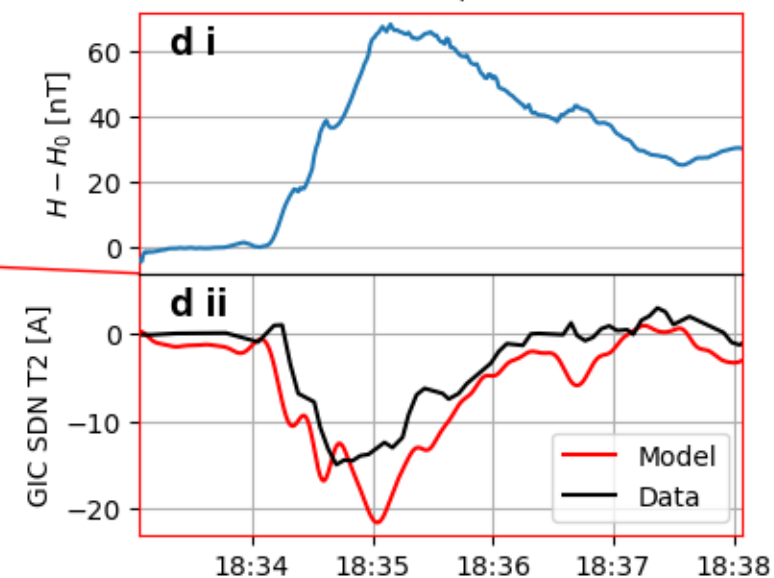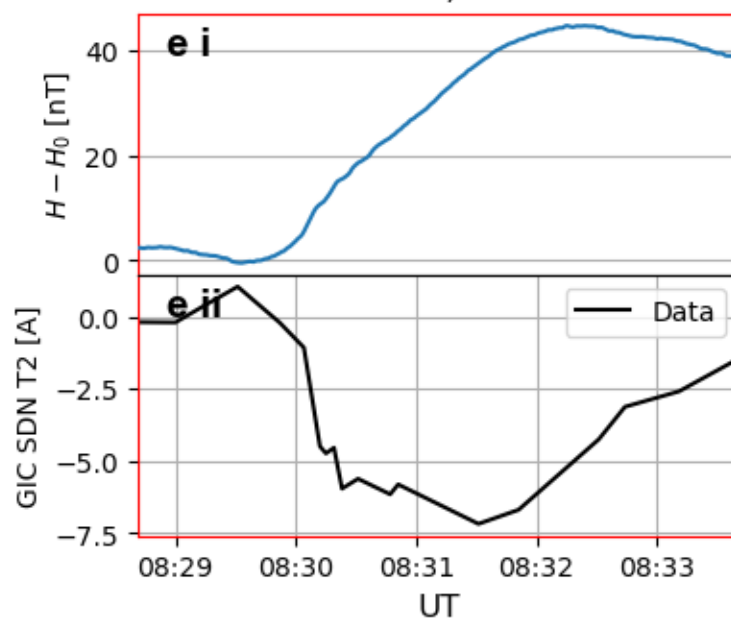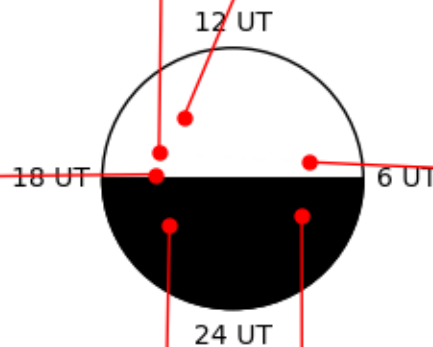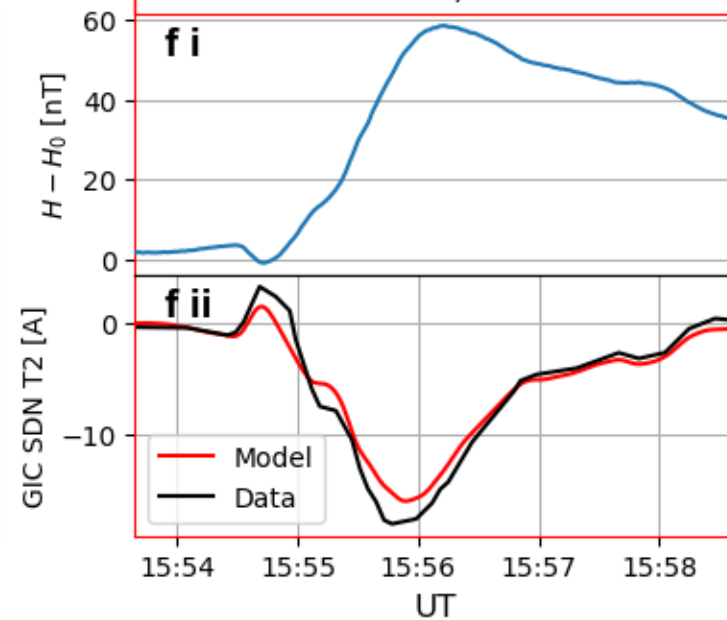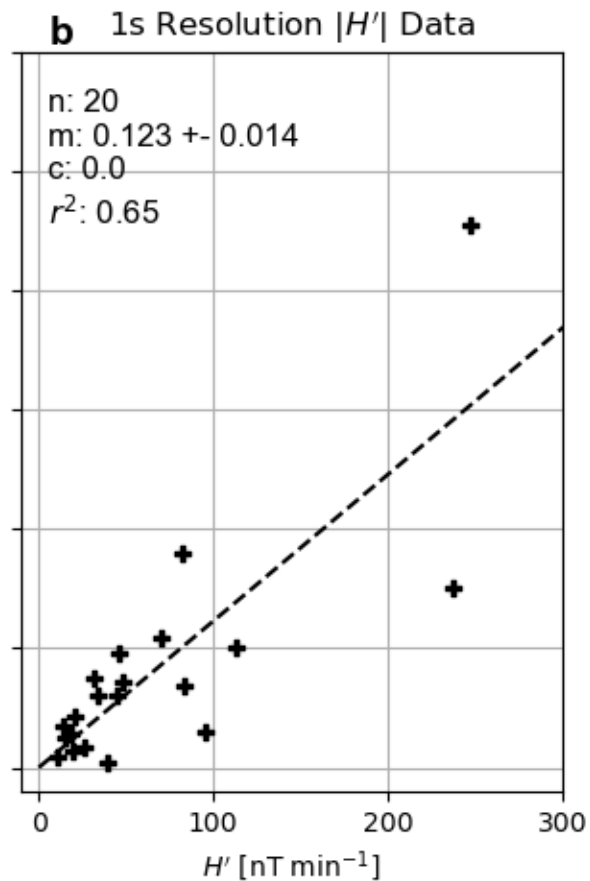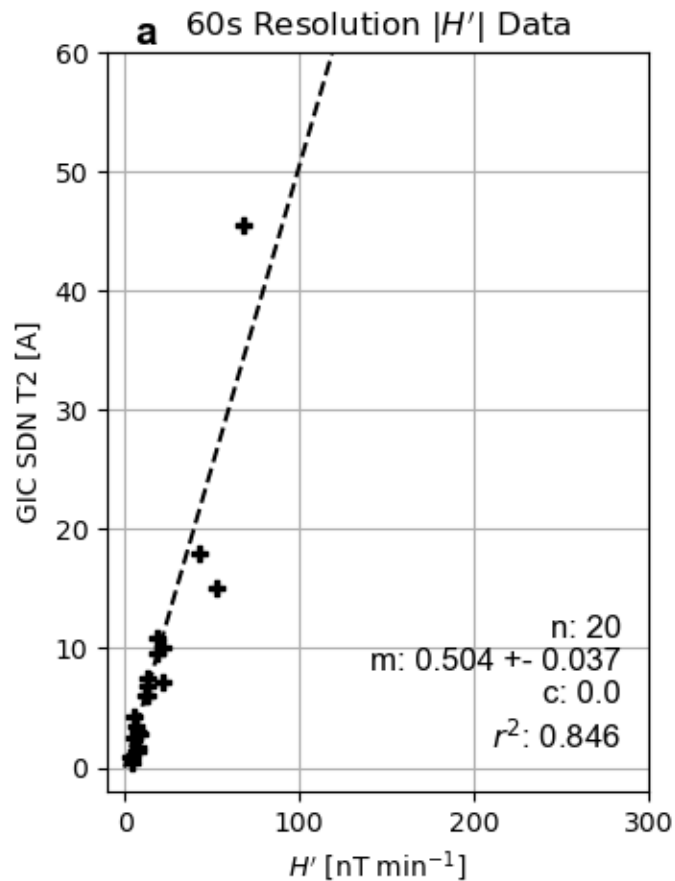
Figure 3.

17-03-2015; MLT: 16.7   22-06-2015; MLT: 17.8

Figure 4.

Figure 5.

a 60s Resolution |H'| Data

n: 20
m: 0.504 +- 0.037
c: 0.0
r^2: 0.845

b 1s Resolution |H'| Data

n: 20
m: 0.123 +- 0.014
c: 0.0
r^2: 0.65

c 1s |H'| Model

n: 20
m: 0.161 +- 0.009
c: 0.0
r^2: 0.928

d

× 60s/Model
● 1s/Model

Figure 6.

Figure 7.

Varying A_{DL} Varying ω Varying θ_{DL}

Figure 8.

a Varying A_{DL}

Legend:
- 10.0
- 34.5
- 55.0

b Varying ω

Legend:
- 0.015
- 0.055
- 0.1

c Varying θ_{DL}

Legend:
- 0.0
- 0.79
- 1.57

GIC [A] vs H' [nT min^{-1}]

Figure 9.

a Varying A_{DL}
b Varying ω
c Varying θ_{DL}
d
e
f

H' [$nT\ min^{-1}$]

$^{GIC}/_{H'}$ [$A\ nT^{-1}\ min$]

A_{DL}

ω

θ_{DL}

Figure 10.

Figure 11.

Figure columns titled: **Varying A_{DL}**, **Varying ω**, **Varying θ_{DL}**
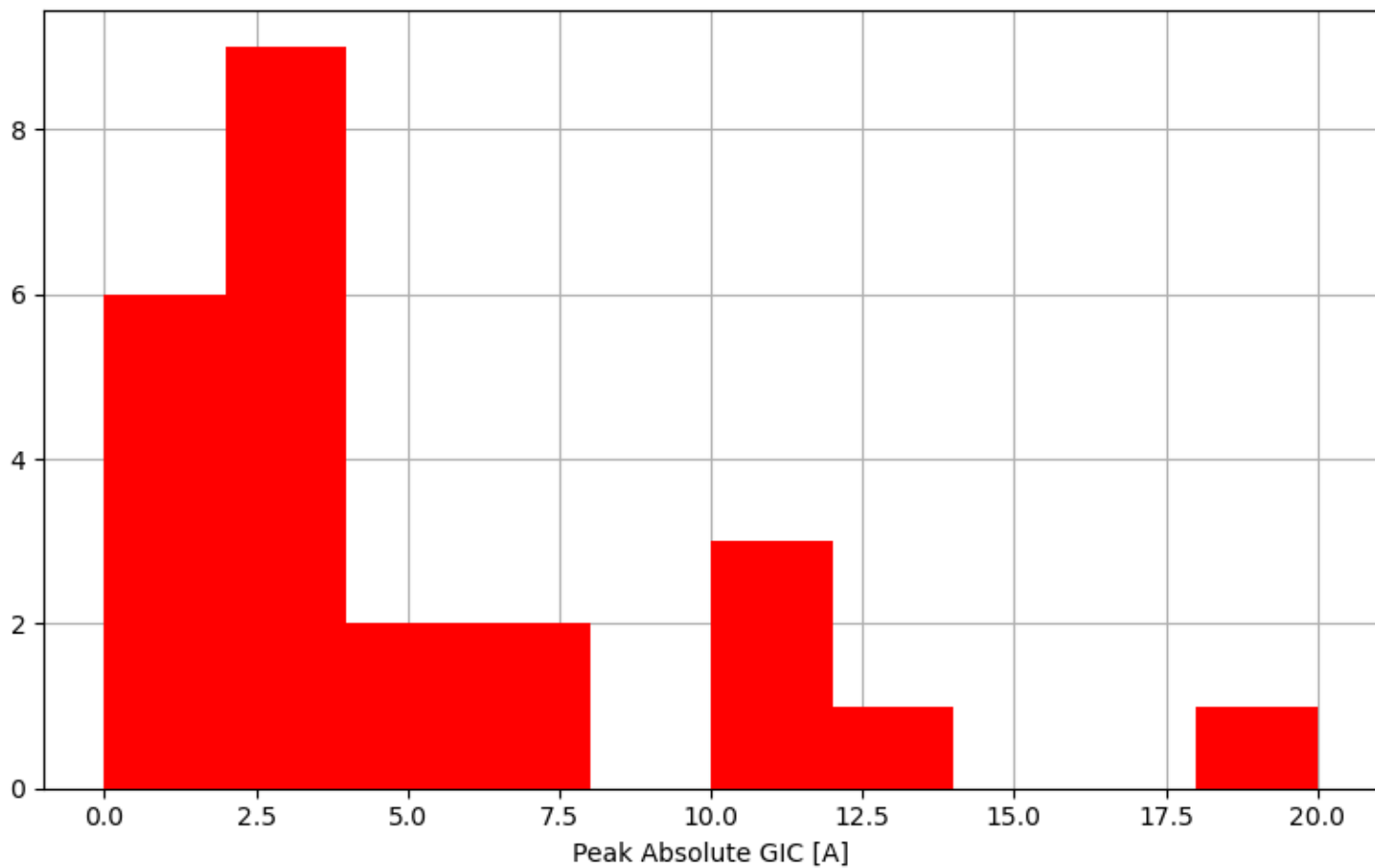
Row labels: **Reducing Parameter** (a, b, c), **Increasing Parameter** (d, e, f)

Y-axis: Number of Transformers

X-axis: GIC Relative to Baseline
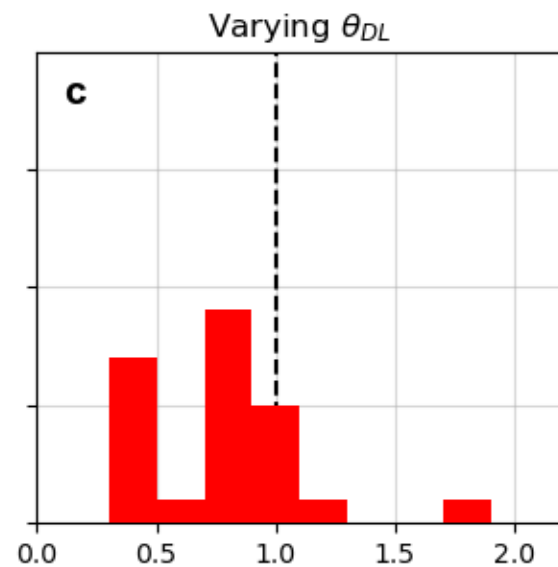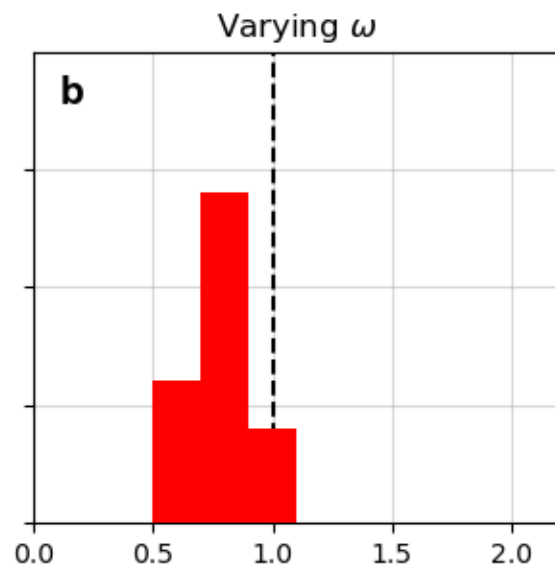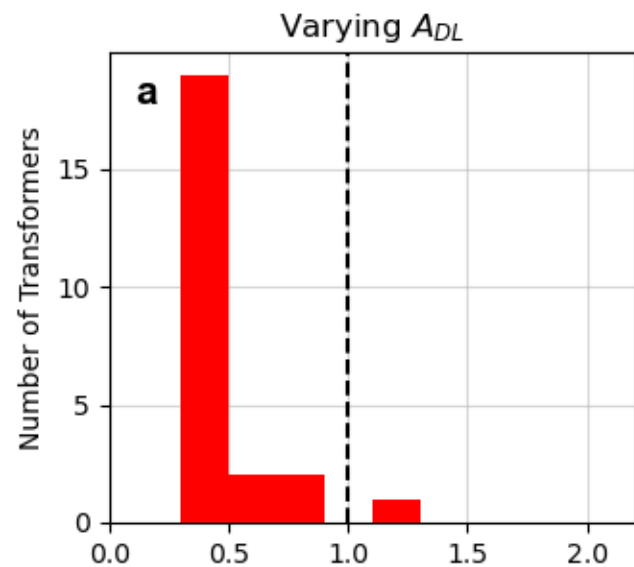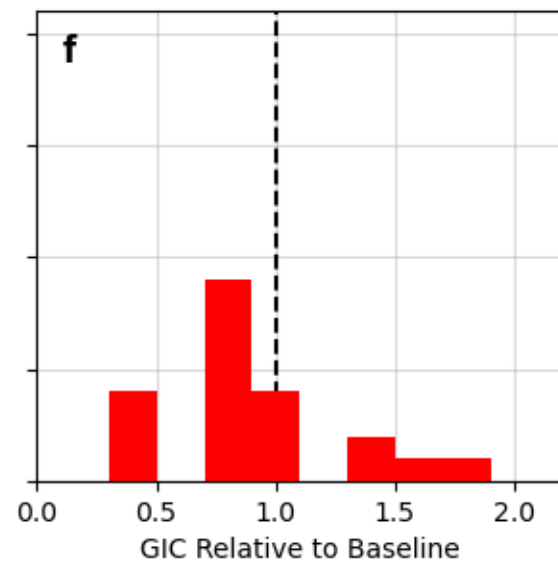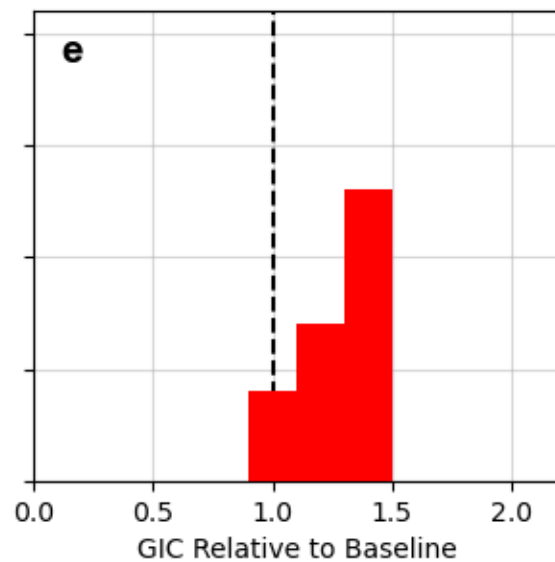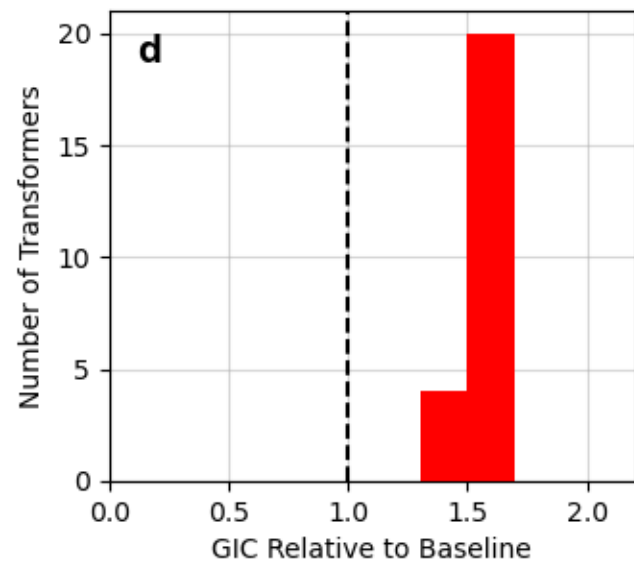
Figure 12.

Baseline Event

Figure 13.

Figure B1.